

Problems of Planetology, Cosmochemistry and Meteoritica

Alexeev V.A. On temporal variations of the intensity of galactic cosmic rays during last billion years: Modelling of the distributions of the cosmic ray exposure ages of the iron meteorites

Vernadsky Institute of Geochemistry and Analytical Chemistry RAS, Moscow

Abstract. Passage of the solar system through the galactic arms may be accompanied by variations in the intensity of galactic cosmic rays (GCR) and by changes in the frequency of meteorite-forming collisions on the parent bodies. For studying these variations during the last billion years, the data about the distribution of the cosmic ray exposure ages of iron meteorites can be used. On the basis of the analysis of the distribution of such ages, it was supposed the presence of variations in the intensity of GCR with a period of ~ 150 million years [Shaviv, 2003]. However, the correctness of this conclusion is disputed [Wieler et al., 2011]. For further study of this question, in this work we compare the parameters of the model distributions of cosmic ray exposure ages with parameters of distributions of cosmic ray exposure ages of iron meteorites.

Key words: cosmic rays, iron meteorites, exposure ages, modeling.

Citation: Alexeev V. A. (2014). On temporal variations of the intensity of galactic cosmic rays during last billion years: Modelling of the distributions of the cosmic ray exposure ages of the iron meteorites. *Experimental geochemistry*. V. 2. No.

The study of variations of the GCR intensity during the last billion years is possible with the attraction of the data about the content in the meteorites of the long-life cosmogenic radionuclide of ^{40}K ($T_{1/2} = 1.277$ billion years) in combination with the data about the content of the cosmogenic radionuclides of ^{36}Cl , ^{26}Al , ^{10}Be and stable isotopes of rare gases [Lavielle et al., 1999; Wieler et al., 2011]. Because of the higher mechanical strength of iron meteorites they are less subjected to destruction at the collisions than the stony meteorites. Therefore iron meteorites, in comparison with the stones, have approximately by an order higher cosmic ray exposure ages (T) – up to billion years and more. As a result, the system of radiation dating by ^{40}K - K gives the potential possibility to study the average flow of cosmic radiation on the long-term scale – over approximately the past 10^9 years. Method is based on the combination of data about the content of cosmogenic radionuclide (^{40}K) and of potassium stable cosmogenic nuclides (^{39}K and ^{41}K) [Voshage, Hintenberger, 1961; Voshage, 1984].

In some studies are found the systematic differences between the ages obtained using pairs radioactive and stable nuclide, such as $^{36}\text{Cl}/^{36}\text{Ar}$, $^{39}\text{Ar}/^{38}\text{Ar}$ and $^{26}\text{Al}/^{21}\text{Ne}$, when compared with $^{40}\text{K}/^{41}\text{K}$ ages (see, e.g. [Lavielle et al., 1999] and references therein). These differences are usually interpreted as evidence of a higher (by ~ 30 - 50%) cosmic ray flux in the past few million years, than the average for a long time, as other explanations, such as erosion in the space, could not satisfactorily explain these differences. However, some iron meteorites have evidences of the complex radiation history, caused by the collision fragmentation of the parent objects of meteorites, which increases uncertainty in the conclusions about variations in the cosmic-ray intensity [Wieler et al., 2011].

Data on cosmic ray exposure ages of the iron meteorites may also be used for establish the proposed periodicity of changes of GCR intensity and the rate of formation of meteorites ~ 150 million years as a result of the periodic passage of the solar system through the spiral arms of the Galaxy [Shaviv, 2002, 2003; Scherer et al., 2006]. The increase of rate of formation of stars and supernovas in the arms leads to the increase of local GCR flux. However, conclusions in these studies frequently are contradictory owing to their dependence on the adopted procedure of the selection of the data about the ages for the subsequent analysis [Wieler et al., 2011; Shaviv, 2003; Scherer et al., 2006].

The present paper presents the results of a comparative analysis of the distributions of cosmic ray exposure ages of iron meteorites. For this purpose, there was used the set of ages for 83 iron meteorites of 13 chemical groups, compiled mainly from data of [Voshage, 1984; Voshage, Feldmann, 1979; Voshage et al., 1983]. An important point at the execution of these studies is the need to avoid (or rather replace on the mean) of the values of cosmic ray exposure ages that can relate to "pair" meteorites (i.e., formed by a single collision with the parent body). To solve such problem at the analysis of the distribution of cosmic ray exposure ages of achondrites (eucrites) Strashnov et al. [2013] used the information criterion of Akaike (AICc) [Akaike, 1974]. We used the same criterion to determine the most probable number of collisions that caused the resulting set of values of cosmic ray exposure ages of iron meteorites of different chemical groups. Thus out of 83 values was compiled set of 28 values of ages, each of which most probably corresponds to the separate event of the formation of iron meteorites. Distribution of initial and corrected sets of ages is shown in Fig. 1. Note that the second distribution, possibly, characterized by two maxima, attributable according to the approximation by the "best" Gaussian curves, towards 280 ± 90 and 720 ± 170 million years.

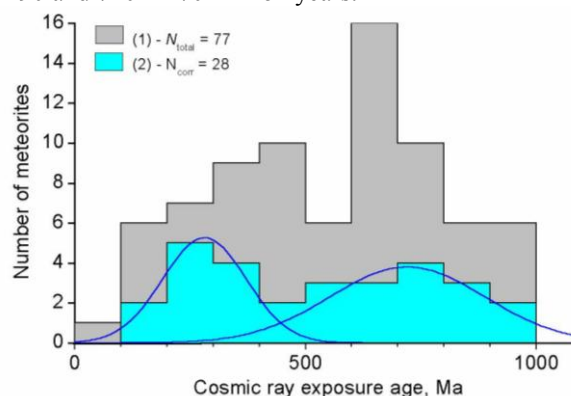


Fig. 1. Distribution of the cosmic ray exposure ages of iron meteorites. (1) - all meteorites with $T < 1200$ Myrs; (2) - meteorites with the ages corrected for possible "paired" falls; approximation is made by the "best" Gaussian curves

Further analysis of the distribution of the corrected values of ages was conducted by calculating the values of the phase (according to [Scherer et al., 2006]) and study of parameters of the distribution of these values of the phase. For each value of the cosmic ray exposure age of meteorite

Abstracts

T was calculated the phase (Ph) according to the ratio $Ph = T / t - \text{int}(T / t)$. Here t is supposed period in the distribution of ages. Value of Ph changes from 0 to 1. Farther, for the selected t value, the selective characteristics of the distribution of the obtained values of the phase were determined: the dispersion S^2 , central moment of m_4 , the index of excess E_k , and also the value of χ^2 [Stepnov, 1985]. In this investigation the analysis was carried out for 17 values of t : 100, 150, 200, 850 and 900 million years. Was further executed the analysis of changes of each of the parameters in the dependence on t .

For the subsequent comparison analogous procedure was executed for the model distributions of cosmic ray exposure ages. With the aid of the developed for this purpose programs were generated 100 and 1000 values of ages, randomly distributed in the interval 0 - 1000 million years without the assumed change in the frequency of the formation of meteorites (mono), and the same number of the meteorite ages, the frequency of appearance of which changed with the period of 150 million years (diff.), taking into account that the intersection of galactic arms is accompanied by a change in the rate of formation of meteorites.

Changes of each of the indicated above parameters in the dependence on t for the model distributions of ages and for distribution of iron meteorite ages are given in Fig. 2 and in the table. From Fig. 2 it is evident that for the model distributions without the assumed alternation in the frequency of the formation of meteorites (100 and 1000, mono) the χ^2 values for all values of t agrees within (1-2) σ with the mean value. However, for the model distributions, in which the frequency of the formation of meteorites was varied with the intended period of $t = 150$ million years (100 and, especially, 1000, diff), the χ^2 values for $t = 150$ million years have been significantly below of average value - on $\Delta = (49 \pm 16)\%$ for $N=100$ and on $(67 \pm 8)\%$ for $N = 1000$. Analogous high Δ values are found for other parameters (see table) for the model distributions of the ages of meteorites with the period of a change in the frequency of their formation $t = 150$ million years (100 and 1000, diff.). For the distribution of 28 corrected ages of meteorites is not observed any significant deviation of any of the parameters from its average value, like and for the distributions of 100 and 1000 (mono).

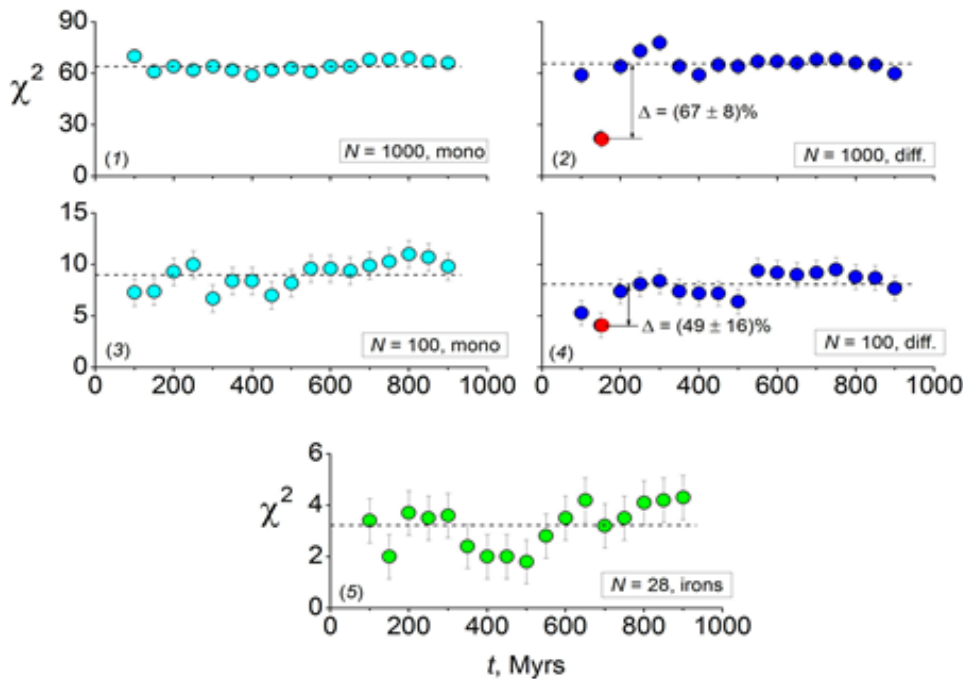


Fig. 2. Values of χ^2 in the distributions of phase $Ph=T/t - \text{int}(T/t)$, depending on the expected period (t) of change of cosmic ray exposure ages (T) of iron meteorites.

(1-4) - dependences for distributions with generation of 1000 (1, 2) or 100 (3, 4) of random values of ages with constant (mono) and variable (diff., modification period $t = 150$ million years) rate of formation of meteorites. (5) - the same for the distribution of the corrected values of cosmic ray exposure ages of meteorites.

Table. Values of the deviation (Δ , %) from the average values of the phase distribution for the magnitude of the proposed periodicity $t = 150$ million years.

Number of events and type of the distribution	S^2	m_4	E_k	χ^2
1000, mono	2 ± 2	1 ± 3	2 ± 3	5 ± 5
1000, diff.	27 ± 5	29 ± 8	43 ± 4	$67 \pm 8^*$
100, mono	1 ± 10	5 ± 14	5 ± 11	18 ± 16
100, diff.	27 ± 10	38 ± 16	24 ± 8	$49 \pm 16^*$
28, Irons	6 ± 16	23 ± 32	12 ± 23	38 ± 28

* See Fig. 2.

This work was supported in part by Fundamental Research Program No. 22 of the Russian Academy of Sciences and by the Program no. 4 of ONZ of Russian Academy of Science.

References

1. Akaike H. (1974). A new look at the statistical model identification. *IEEE T. Automat. Contr.* AC-19, no. 6, p. 716-723.
2. Lavielle B., Marti K., Jeannot J.P., Nishiizumi K., Caffee M. (1999). The ^{36}Cl - ^{36}Ar - ^{40}K - ^{41}K records and cosmic ray production rates in iron meteorites. *Earth Planet. Sci. Lett.*, v. 170, p. 93-104
3. Scherer K., Fichtner H., Borrmann T., Beer J., Desorgher L., Flukiger E., Fahr H.J., Ferreira S.E.S., Langner U.W., Potgieter M.S., Heber B., Masarik J., Shaviv N.J., Veizer J. (2006). Interstellar-terrestrial relations: variable cosmic environments, the dynamic heliosphere, and their imprints on terrestrial archives and climate. *Space Sci. Rev.*, v. 127, p. 327-465

4. Shaviv N.J. (2002). Cosmic ray diffusion from the galactic spiral arms, iron meteorites, and a possible climatic connection. *Phys. Rev. Lett.*, v. 89, art. no.-089901.
5. Shaviv N.J. (2003). The spiral structure of the Milky Way, cosmic rays, and ice age epochs on Earth. *New Astron.*, v. 8, p. 39–77
6. Stepanov M.N. (1985). Statistical methods for processing the results of mechanical tests: Handbook. - M.: Mashinostroenie.-232 p. (In Russian)
7. Strashnov I., Bland P.A., Spurny P., Towner M.C., Gilmour J.D. (2013). Times of impacts that deliver samples of Vesta to Earth derived from ultrasensitive ⁸¹Kr-Kr cosmic ray exposure age analysis of Eucrites. *Geochim. Cosmochim. Acta*, v. 106, p. 71-83.
8. Voshage H. (1984). Investigations of cosmic-ray-produced nuclides in iron meteorites, 6. The Signer-Nier model and the history of the cosmic radiation. *Earth Planet. Sci. Lett.*, v. 71, p. 181–194.
9. Voshage H., Feldmann H. (1979). Investigation on cosmic ray produced nuclides in iron meteorites, 3. Exposure ages, meteoroid sizes and sample depths determined by mass spectrometric analyses of potassium and rare gases. *Earth Planet. Sci. Lett.*, v. 45, p. 293-308.
10. Voshage H., Feldmann H., Braun O. (1983). Investigation on cosmic ray produced nuclides in iron meteorites, 5: More data on the nuclides of potassium and noble gases on exposure ages and meteoroid sizes. *Z. Naturforsch.*, v. 38a, p. 273-280
11. Voshage H., Hintenberger H. (1961). Massenspektrometrische Isotopenhäufigkeitsmessungen an Kalium aus Eisenmeteoriten und das Problem der Bestimmung der ⁴¹K-⁴⁰K-Strahlungsalter. *Z. Naturforsch.*, v. 16a, p. 1042–1053
12. Wieler R, Beer J., Leya I. (2011). The galactic cosmic ray intensity over the past 10⁶–10⁹ years as recorded by cosmogenic nuclides in meteorites and terrestrial samples. *Space Sci Rev.*, v. 176, p. 351-363.

Alexeev V.A., Kalinina G.V., Pavlova T.A. Track study of Chelyabinsk LL5 and Košice H5 chondrites

Vernadsky Institute of Geochemistry and Analytical Chemistry
RAS, Moscow

Abstract. Measurements and the analysis of distributions of density of *VH*-nuclei tracks of cosmic rays in olivine crystals of ordinary chondrites of Chelyabinsk LL5 (fall on February, 15th, 2013) and Košice H5 (fall on February, 28th, 2010, Slovakia) were carried out. About 40% of crystals from the Chelyabinsk meteorite is characterised by high density of tracks – 10⁵-10⁶ cm⁻² up to 10⁷ cm⁻², whereas density of tracks in other crystals is essentially more low – less 5×10² cm⁻². The obtained data confirms a conclusion [Galimov et al., 2013] about a complex shock-thermal and radiation history of the Chelyabinsk meteorite. The density of tracks in the majority of olivine crystals from the Košice meteorite lies in the range of 10⁴-10⁶ cm⁻²; average value is equal 1.5×10⁵ cm⁻².

Key words: cosmic ray tracks, meteorites, Chelyabinsk, Košice.

Citation: Alexeev V.A., G.V. Kalinina, T.A. Pavlova (2014). Track study of Chelyabinsk and Košice chondrites. *Experimental geochemistry*, V. 2. №9

In studying the radiation and shock-thermal histories of meteorites, important information can be derived by examining their material by track analysis. The main sources of the tracks observed in the meteorites are the nuclei of the iron-group elements (*VH*-nuclei, 23<*Z*<29), which form part both of contemporary galactic (GCR) and solar (SCR) cosmic rays, and into the composition of the cosmic radiation, which existed at the early stage of the formation of the solar system. Depending on the shock-thermal history of meteoritic material, traces of nucleus stopping in silicate minerals may be partly or completely lost. On the one hand, this extremely complicates interpreting of the results but, on the other hand, makes it possible to record parameters of the tracks that were produced at various stages of the radiation history of meteorites. The earliest stage when tracks were generated was the preaccretion evolutionary period of the parent bodies of meteorites, when tiny crystals in them could be irradiated in the gas-dust protoplanetary nebula by locally accelerated ions of iron group elements in solar wind [Kashkarov, 1988; Kashkarov, Ustinova, 2000]. Later meteoritic material that occurred near or at the surface of the regolith of the parent body was irradiated, depending on the thickness of the shielding layer of the regolith material, by *VH* nuclei of GCR and SCR [Kashkarov, 1988; Caffee et al., 1987]. The third stage of irradiation started when meteorites were produced, when the accumulation rate of the tracks of *VH* nuclei from GCR depended on the depth from the surface of the meteoroid at which the crystals occurred, and the density of the tracks was directly proportional to the cosmic-ray exposure age [Bhattacharya et al., 1973].

The realized previously track studies of meteorite Chelyabinsk showed the complex radiation-thermal history of this meteorite [Galimov et al., 2013]. For obtaining further information about this unique meteorite, we conducted track studies of samples no. 10-85 (33.3 g.) and no. 10-64 (10.4 g.), M.A. Nazarov provided samples. We are executed also track studies of the samples of the Košice meteorite. This meteorite fell out on February 28, 2010 in Slovakia, near city Košice. In total, more than 150 fragments of meteorite were collected by overall mass about 9 kg. [Borovička et al, 2013]. A preatmospheric radius of this meteorite is evaluated as *R*~40-45 cm [Povinec et al., 2013]. The samples of this meteorite for studies were provided by Prof. P. Povinec (Comenius University, Bratislava, Slovakia).

Parameters of the tracks were measured in microcrystals of olivine grains of the size fraction 50–200 μm. A few dozen grains of olivine suitable for track studies were handpicked from 0.5- to 1-g samples. The selected grains were packed into epoxy pellets, which were then polished and chemically etched in a solution of the WN type, which was specially designed for the effective selective distinguishing of tracks in olivine [Krishnaswami et al., 1974]. We examined 59 and 24 grains of olivine in the Chelyabinsk and Košice chondrites, respectively. The measured track densities in olivine grains from these chondrites are presented in the form of histograms in Fig. and in the Table. As can be seen from them, the distributions of the densities are different for these chondrites.

All investigated crystals of olivine from the Chelyabinsk meteorite can be divided into two groups.

Abstracts

The first group consists of crystals with high density of tracks, and the second group consists of crystals in which the tracks were not found. (It is essential to note the fact, the distributions of crystals according to the sizes in each

group are identical to each other with average size of ~ 100 μm .) The average density of tracks in the grains of the first group was $\rho_{\text{av}} \sim 4.7 \times 10^5 \text{ cm}^{-2}$ (Fig.).

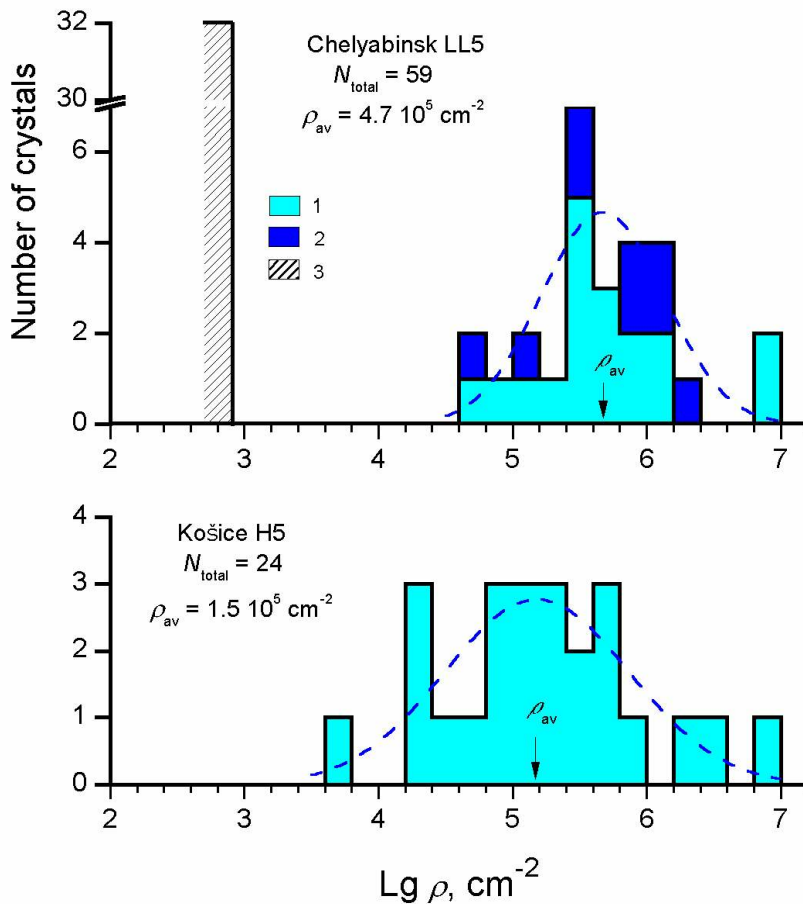


Fig. Distribution of the track density (ρ) of the *VH*-nuclei of cosmic rays in the olivine crystals of the chondrites of Chelyabinsk

1 - sample no. 10-65;
 2 - sample no. 10-64;
 3 - the crystals without tracks) and Košice (sample no. 57).

N - number of investigated crystals.

Table. Track parameters in the microcrystals of olivine from the Chelyabinsk and Košice chondrites and the shielding depth of the investigated samples from the preatmospheric surface of meteorites.

Meteorite, type	Number of crystals	Total area*	Track density**, cm^{-2}	Shielding depth, cm
Chelyabinsk LL5	27	202	$(4.7 \pm 1.1) \times 10^5$	$\sim 3 \pm 1$
	32	497	$< 5 \times 10^2$	> 23
Košice H5	24	330	$(1.5 \pm 0.4) \times 10^5$	$(11 \pm 1)^{***}$

Notes: * In area units per one grid cell of the microscope ($4 \times 10^{-6} \text{ cm}^2$); ** Average track density for all microcrystals of every sample; *** Under the assumption: the cosmic-ray exposure age $t = 6 \text{ Ma}$.

The values of the density of tracks in most grains of the Chelyabinsk chondrite lie at the interval of $\sim 10^5$ - 10^6 cm^{-2} , up to 10^7 cm^{-2} . If tracks in these grains were accumulated from the *VH*-nuclei of GCR in the preatmospheric body of chondrite during its cosmic-ray exposure age, i.e., after its isolation from the parent body of $\sim 1.2 \text{ Ma}$ [Haba et al., 2014], the shielding depth of these grains must be only $d \sim 3 \text{ cm}$ from the preatmospheric surface of meteorite, according to the calculated dependences [Bhattacharya et al., 1973]. The probability of retaining the samples from such small depth of meteorite with a preatmospheric radius of $R \sim 10 \text{ m}$ after the losses of the substance because of splitting, ablation and scattering during the passage of the earth's atmosphere is close to zero. It is most probably, tracks with so high a density could be formed during irradiation of the olivine microcrystals at the regolithic stage of the formation of this meteorite parent body due to the irradiation by *VH*-

nuclei of SCR on the very body surface as this considered above. A similar conclusion was made earlier according to the results of track studies of other samples of the Chelyabinsk meteorite [Galimov et al., 2013]. The significance of this assumption is confirmed by the absence of tracks in the crystals from second group. Thus, for instance, in the sample no. 10-85 of the Chelyabinsk chondrite the tracks were not discovered in $\sim 60\%$ of olivine grains (31 of 49). The upper limit of the track density for such samples is evaluated as $5 \times 10^2 \text{ cm}^{-2}$. This value corresponds to the shielding depth of $d > 23 \text{ cm}$ in the preatmospheric body of the meteorite.

In the Košice H5 meteorite (sample no. 57) the track density in the majority of the olivine crystals lies at the interval of 10^4 - 10^6 cm^{-2} ; the average value is $\rho_{\text{av}} = 1.5 \times 10^5 \text{ cm}^{-2}$ (Fig.). Because of the absence of information about the cosmic-ray exposure age of Košice meteorite, it is no possibility to determine the shielding depth d of the

investigated sample in the meteorite according to the track density. However, it is possible to make a crude estimate of d value. It is known, the distribution of the cosmic-ray exposure ages of H-chondrites is characterized by peak in the region of 3-9 Ma (for example, [Alexeev, 2005]). This peak enclose about 50% of all age values of the H-chondrites (falls). In this case, for fifth petrologic type of H-chondrites, this includes the Košice meteorite, this value noticeably higher: ~57%. The maximum of the peak of ages is fallen on ~6 Ma.

If we accept for Košice meteorite the cosmic-ray exposure age $t = 6$ Ma, the obtained track density will correspond to the shielding depth $d = 11 \pm 1$ cm of the investigated sample. For the age values $t = 3$ or 9 Ma, the d value will be equal to 9 ± 1 or 13 ± 1 cm, respectively. So, it is possible to consider as the great probability, the sample no. 57 of the Košice meteorite was located in the deposition depth of ~9 - 13 cm in the preatmospheric body.

The authors are grateful to M.A. Nazarov and P. Povinec for providing the meteorite samples.

This work was supported in part by Fundamental Research Program no. 22 of the Russian Academy of Sciences and by the Program no. 4 of ONZ of Russian Academy of Science.

References:

1. Alexeev V.A. (2005). The History of Ordinary Chondrites from the Data on Stable Isotopes of Noble Gases (a Review). *Solar System Research*, v. 39, no. 2, p. 124–149.
2. Bhattacharya S.K., Goswami J.N., Lal D. (1973). Semiempirical rates of formation of cosmic ray tracks in spherical objects exposed in space: pre- and post-atmospheric depth profiles. *J. Geophys. Res.*, v. 78, no. 34, p. 8356-8363.
3. Borovička J., Tóth J., Igaz A., Spurný P., Kalenda P., Haloda J., Svoreň J., Kornoš L., Silber E., Brown P., Husárik M. (2013). The Košice meteorite fall: Atmospheric trajectory, fragmentation, and orbit. *Meteoritics & Planetary Science*, v. 48, p. 1757–1779. doi: 10.1111/maps.12078.
4. Caffee M.W., Hohenberg C.M., Swindle T.D., Goswami J.N. (1987). Evidence in meteorites for an active early sun. *Astrophys. J.*, v. 313, no. 1, p. L31-L35.
5. Galimov E.M., Kolotov V.P., Nazarov M.A., Kostitsyn Yu.A., Kubrakova I.V., Kononkova N.N., Roshchina I.A., Alexeev V.A., Kashkarov L.L., Badyukov D.D., Sevast'yanov V.S. (2013). Analytical Results for the Material of the Chelyabinsk Meteorite. *Geochemistry International*, 51, no. 7, p. 522–539.
6. Haba M.K., Sumino H., Nagao K., Mikouchi T., Komatsu M., Zolensky M.E. (2014). Noble gases in the Chelyabinsk meteorite. *Abstracts of the 45th Lunar and Planetary Science Conference*, #1732.pdf
7. Kashkarov L.L., G.K. Ustinova (2000). Radiation Characteristics of the Situation in the Early Solar System. *Dokl. Ross. Akad. Nauk*, v. 372, no. 5, p. 659–662.
8. Kashkarov L.L. (1988). High-Energy Nuclei of VH-Group Cosmic Rays in the Early Solar System, *Izv.*

Akad. Nauk SSSR, Ser. Fiz., v. 52, no. 12, p. 2321–2324.

9. Krishnaswami S., Lal D., Prabhu N., Tamhane A.S. (1974). Olivines: revelation of tracks of charged particles. *Science*, v. 174, no. 4006, p. 287–291.
10. Povinec P.P., Masarik J., Sýkora I., Laubenstein M., Beňo J., Kováčik A., Porubčan V. (2013). Cosmogenic nuclides in Košice meteorite. *Abstracts of the 76th Annual Meteoritical Society Meeting*, #5067.pdf

Barenbaum A.A. Tectonic - Magmatic Consequences of Fallings of Galactic Comets on Terrestrial Planets

Oil and Gas Research Institute RAS, Moscow

Abstract. With the use of the author's theoretical model are discussed geological structures, creating of which can be explained by fallings of galactic comets on terrestrial planets: Mercury, Mars, Earth, Venus and the Moon. The model predicts that, depending on combination of a number of conditions, galactic comets may form on these planets following types of structures: craters, diatremes, lava sheets, volcanoes, dome-shaped surface uplift, as well as crown and Montes (on Venus). The main factors that influence on origin of these structures on planets are: 1) density of gas shell, 2) thickness of planetary lithosphere, 3) composition and degree heating of lithosphere rocks, 5) frequency of fallings galactic comets. We are discussing specific features of these structures on the Moon, Mars, Earth and Venus.

Key words: Galactic comets, shock waves, tectonic-magmatic processes, craters, diatremes, volcanoes, asthenospheric lens.

Citation: Barenbaum A. A. (2014). Tectonic-magmatic consequences of fallings of galactic comets on terrestrial planets, *Experimental geochemistry*. V. 2. No

Introduction. Origin on terrestrial planets of homogenous geological structures (continents, seas, volcanoes, mountains, craters, etc.) is the issue in Planetology, which is yet very far from adequate explanation. Things began to change for the better due to the recent discovery of phenomenon of jet expiration of gas-dust substance from Galactic center. When fact of fallings galactic comets at Solar system planets was open [Barenbaum, 2002], and physical mechanism of interaction of these comets with Earth's atmosphere and lithosphere began to be studied theoretically [Barenbaum, 2013].

Author's investigations have shown that these geological structures may be caused fallings of galactic comets. The physical mechanism of formation of these structures on all planets apparently is universal, and all their differences are determined by four factors: 1) density of gaseous envelope, 2) thickness of planetary lithosphere, 3) degree of heating and composition of lithosphere rocks, and 4) intensity of fallings large cosmic bodies, especially of galactic comets.

In this paper, we wish to discuss the interaction mechanism of galactic comets with atmosphere and lithosphere planets. We also analyze the specificity of action this mechanism with respect to formation of craters, diatremes, lava sheets, shield volcanoes, and other leading types of surface topography on atmosphereless Moon, Mercury and Mars that has a very tenuous gas shell, as well Earth and Venus with a sufficiently dense atmospheres. But first, we will need to briefly describe

some properties of galactic comets [Barenbaum, 2002, 2010].

Information about Galaxy's comets. Galactic comets are a newly opened class of major space bodies, which move in the galactic plane and cyclically bombard all planets of the Solar system solely at the moments when Sun is located in the jet flows and the spiral arms of Galaxy. Those periods are repeated at 20-37 million years and have duration of 1-5 million years old. Therefore, fallings of galactic comets have character of relatively short "cometary showers". Effects of such showers are most studied for our planet. Found that during a one bombardment to the Earth may fall of $\sim 10^4 \div 10^7$ galactic comets. All those periods for the last 560 million years Earth's history are fixed by geologists in form of boundaries straton Phanerozoic geologic time scale [Barenbaum et al, 2002, 2004].

Last cometary shower "medium intensity" took place at 5.0- 0.7 million years ago, at the border of Neogene and Quaternary. We estimated that in this time $\sim 3\text{-}5$ galactic comets could to fall on square size $100 \times 100 \text{ km}^2$ [Barenbaum, 2012]. The cometary bombardment caused significant heating of lithosphere rocks that led to a marked lifting of the continents surface. This phenomenon was named "newest uplift crustal" [Artyushkov, 1994]. It is known that along with the continents sharply intensified tectonic-magmatic processes and on the oceans floor [Barenbaum, 2013d, 2013f].

Diameter nucleus of galactic comets is from 100 m to 3.5 km; their mass varies from 10^{12} to 10^{17} g and the kinetic energy from 10^{20} to 10^{25} J. Cometary substance is composed at 80-90% of water ice and at 10-15% of carbon-bearing components. Substance density is $\approx 1.0 \text{ g/cm}^3$. Speed of movement comets of last shower relative to the Sun was close to 450 km/s. In contrast to asteroids and comets of Solar system, galactic comets are

characterized by exponential distribution by diameter, mass and energy, which causes an exponential distribution by sizes of geological structures created by their fallings on planets. Another difference is that due to inclination of the ecliptic at angle 62° to Galaxy plane, the last time comets bombed southern hemispheres of terrestrial planets. Therefore leading landforms of Southern and Northern hemispheres of these planets are differ significantly.

And finally we should say that galactic comets cannot be visually detected by means of astronomy currently. Therefore all that is known about them today we obtained by studying consequences falling of these comets to Earth and other planets as well as results of their collisions with bodies of asteroid belt [Barenbaum, 2010].

Interaction mechanism of galactic comets and planets. We have studied this mechanism in application to Earth as three-step process [Barenbaum, 2013]. In the first step – in Earth's atmosphere – comet nucleus is transformed into peculiar gas-fluid jet consisting of cometary material, subjected to ablation, and shock-heated air [Barenbaum Shuvalov, 2007]. In the second stage this jet inelastically bumps into solid surface, creating narrow-directed hypersonic shock wave which penetrates deep into lithosphere planet and causes heating of cylindrical column of her rocks. Effect of heating is so great that rocks top part of column are vaporized, forming crater. And material under crater is melted, forming magma chamber. When calculating effects of heating rocks by shock wave we used the hydrodynamic model MA Lavrentiev of first approximation [Lavrentiev, 1959; Lavrentiev, Shabat, 1977] designed to study the collisions of bodies with cosmic speeds.

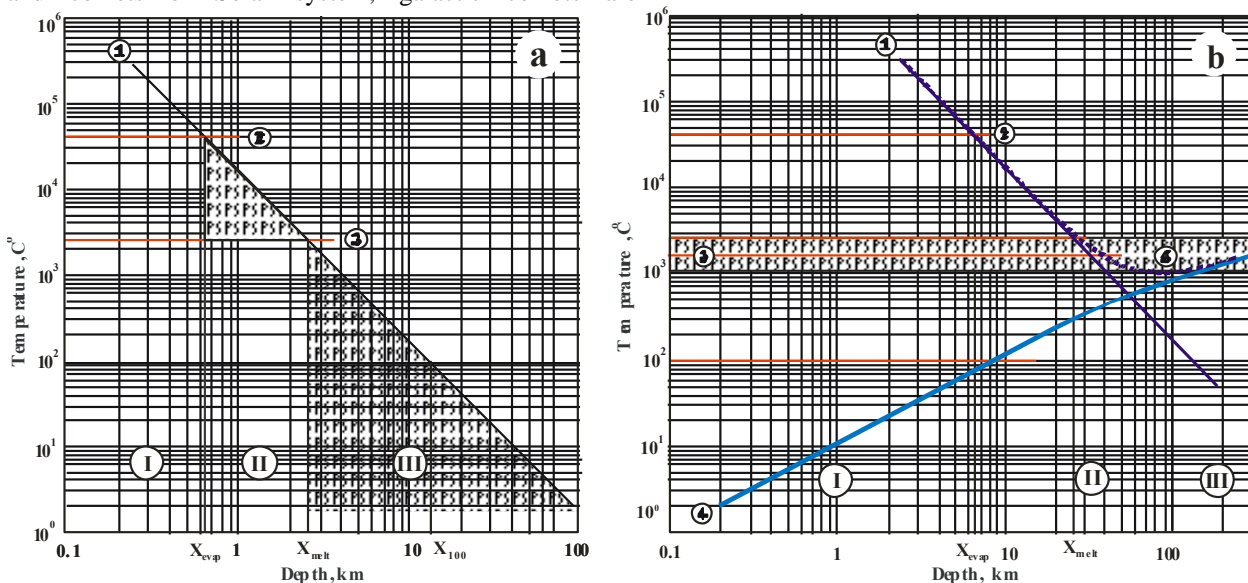


Fig. 1. Heating of lithosphere rocks by shock waves from comets with a diameter nucleus of 300 m (a) and 3000 m (b):

1 – design temperature heating rocks, 2 – evaporation temperature of rocks, 3 – temperature range of melting of rocks (shaded), dotted line – average melting point of 1750, 4 – natural temperature increase with depth for the continental lithosphere, 5 – cumulative heating of rocks. Heating zones rocks: I – evaporation zone (crater), II – melting zone (magma chamber), III – heating zone, IV – asthenosphere; H_{ev} , H_{melt} and X_{100} – respectively the lower boundaries of the zones of evaporation, melting and heating to a temperature of 100°C

In the third stage heat is redistributed in system. The melt rocks which arisen in magma chamber fills crater while its excess can to flow out to surface. If heating energy is not enough, magma crystallizes in upper crust, forming during cooling the intrusives of different composition and structure. If heat energy is not enough magma crystallizes in the upper crust, forming during the cooling the intrusives of different composition and structure. Heating time rocks column by shock wave takes split second, and the time of redistribution and dissipation of heat energy in it takes ~400 thousand years for comets small size and ~2 million years for largest comets.

Heat effects created by shock waves from galactic comets “small” – 300 m and a “large” – 3 km in diameter are illustrated in Fig. 1.

According to our calculations, “small” comets are able to create craters of deep to ~1 km, whereas “large” comets – to 7 km and more. At that, magma chambers created by small comets are located at a depth of ~1-3 km from the surface, and at this case the melt that has been formed in

magma chamber is not completely fills crater. The large comets may create cameras, which reach of asthenosphere depth 100-250 km. In result the large amount of magma can flow to surface. In both cases crater depth coincides with diameter of column heated rocks. On the results base of simulation processes of destruction galactic comet in Earth's atmosphere, we assumed that column diameter is equal to twice diameter of cometary nucleus.

Results of calculations (Fig. 1) are applicable also for comets falling in ocean. From the energy point of view the energy losses due to evaporation of water at crater formation are small (~1-10%). Therefore, for large comets the size of magma chamber stays almost same, and crater depth decreases.

Density of gas shell. Influence of atmosphere and its density we discuss on the basis of analysis of distributions impact craters of diameters $D = 10\div 200$ km on the continental parts of surface of the Moon, Mercury, Mars, Earth and Venus (Fig. 2).

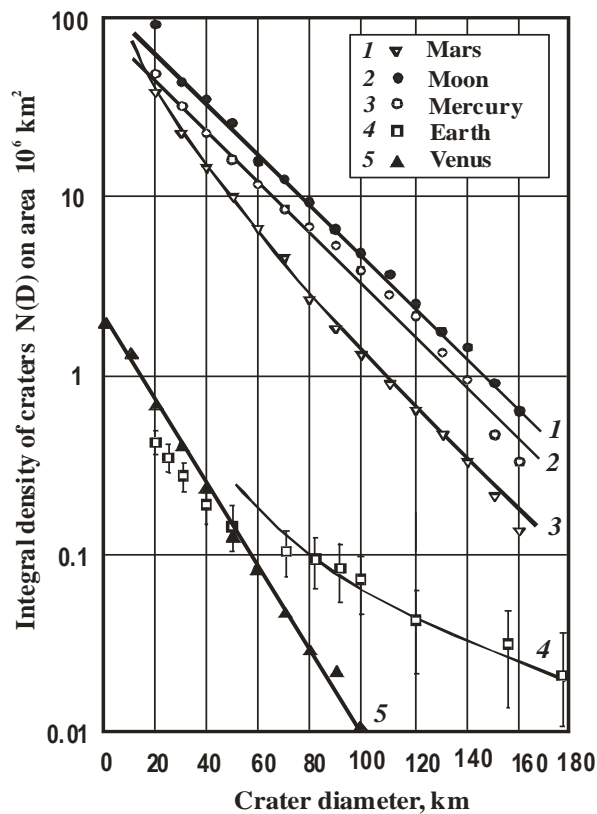


Fig. 2. Integral density of craters on the Moon (1), Mercury (2), Mars (3), Earth (4) and Venus (5). Curve (4) corresponds to inversely-quadratic dependence. Distribution of 1, 2, 3 are based on the data [Kazimirov et al, 1980]; distribution of 4 – builted according to data VI Feldman [Barenbaum, 2010], and distribution of 5 – according to data [W/List of craters on Venus]

Unlike Earth vast majority of craters on other planets and Moon were created by galactic comets. On atmosphereless Moon and Mercury craters distribution $N(D)$ obey by an exponential dependence, which reflects the exponential distribution of diameters of cometary nuclei. In Martian rarefied atmosphere function $N(D)$ is

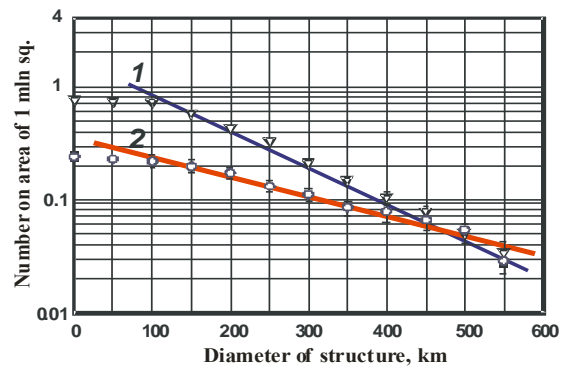


Fig. 3. Integral density on Venus coronae (1) [W/List of coronae on Venus] and montes (2) [W/List of montes on Venus]

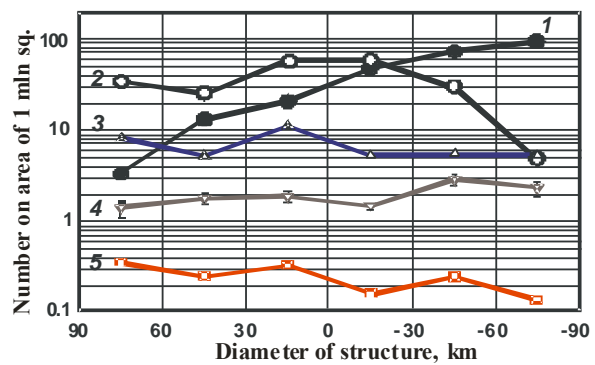


Fig. 4. The density of craters (1, 2, 3), coronae (4) and montes (5) on Mars (1, 2) and on Venus in the latitude belts with step $\Delta\phi = 30^\circ$. Craters on Mars have been formed by fallings of galactic comets (1) and of asteroids and comets of Solar system (2)

deformed. Due to fragmentation of cometary nuclei in atmosphere of Mars number craters of large sizes decreases, and vice versa, number craters small diameters grows.

Due to the high intensity of the last cometary bombardment when density fallings of galactic comets

was ~5 bodies at area $100 \times 100 \text{ km}^2$ [Barenbaum 2012] currently continents of Mercury, Moon and Mars are completely saturated with craters $D \geq 10 \text{ km}$. This saturation limit for all planets is the same and equals to ≈ 100 craters on 10^6 km^2 [Barenbaum, 2002].

In Earth atmosphere the nuclei of galactic comets are destroyed entirely [Barenbaum, 2002]. As a result the cometary craters of $D \geq 10 \text{ km}$ on our planet are absent, and all craters of such size are created asteroids. Their distribution $N(D)$ corresponds to the inverse square law which is intrinsic to large asteroids and comets of Solar system. This dependence for craters on a plot of $D < 80 \text{ km}$ however is distorted by observational selection.

In more dense gaseous envelope Venus the galactic comets are destroyed even more so. Nevertheless they do create large craters. But there are two peculiarities: 1) number of these craters in ~ 100 times less than at atmosphere absence or its low density and 2) their size distribution $N(D)$ has the same exponent index as dependence of Mars in its initial portion. Thus firstly atmosphere significantly reduces energy of cometary gas jet which reaches Venus surface. And secondly mechanism of craters formation in these conditions has its own specifics.

Thickness lithosphere and temperature heating of rocks. We discuss the influence of these factors in two different cases when galactic comets fall on continents or into World Ocean. In the first case (Fig. 1-a) asthenosphere is deep then most comets can create in column of heated rocks three zones: crater (I), magma chamber (II) and the heating zone below the melting point of rocks (III).

In the event of fall comet into the World Ocean where asthenosphere is closer to Earth surface the zone (III) may absent (Fig. 1-b). As a result will be created continuous conductive pipe – “plume” through which magma can flow to the surface from asthenosphere. At that importantly to note that these plumes may be created not only by large comets but also small which are in the vast majority.

Obviously there are other differences. We note only one thing in common for the Earth and other planets. Specificity of falls comet on Earth surface with a “thick” lithosphere is that magma is generated not enough to fill cavity of crater. In result are created a structure which we define [Barenbaum, 2013b] as a kimberlitic pipes or otherwise words diatremes. Approximately 5% pipes contain diamonds and so they geologically well are studied. It is believed that diamond-bearing pipes arise in explosions at depths greater than 100 km [Milashev, 1984].

It is empirically detected [Clifford, 1966] that kimberlitic pipes meet only on the ancient “thick” platforms. In the oceans where diatremes create it would seem easier they are absent. The physical mechanism origin of diamond-bearing pipes also is poorly understood [Milashev, 1984].

However, problematic issues physics diatremes can be solved on the basis of discussed mechanism heating rocks by shock waves [Barenbaum, 2013b]. From the standpoint of given mechanism all diatremes (kimberlitic pipes) can be considered a form of intraplate magmatism which occupies an intermediate position between outpouring of lava on Earth surface and cooling lava in cavity of crater.

We attribute the formation of craters on Venus with this type magmatism.

Consequences fallings of galactic comets on “thin” lithospheric plates in particular into World Ocean are of a different nature. In this case much more quantity magma arises. This magma can reach surface where take part in formation of seamounts and hotspots in marine conditions and trapean outpourings in continental conditions [Barenbaum, 2010, 2011]. Based on these representations the author discusses the issues of intraplate magmatism and modern structure of ocean crust [Barenbaum, 2013a, 2013c] as well as analyzes tectonic-magmatic processes in an oceans caused the latest and several previous cometary bombardments [Barenbaum, 2013, 2013d, 2013i, 2013f].

In addition falling of galactic comets into oceans also leads to appearance in water column of hollow channel with diameter $\sim 0.2\text{-}7 \text{ km}$. This channel fast is filled with water from above and below the magma, that causing powerful benthic processes [Barenbaum, 2013i]. In some places they lead to mixing of the sedimentary rocks and basalt layers of the oceanic crust. As a result the sedimentary interbeds turn out within basaltic foundation, as and diabase sills and fragments of basalt in lower part sedimentary cover of oceanic crust [Panaev, Mitulov, 1993; Blyuman, 2011].

Intensity cometary fallings. Processes of intraplate magmatism caused by massive fallings galactic comets are very complex and diverse. They can be explored only on well-studied geological objects. We will discuss them on example of two such structures: basalt plateau Dariganga in Mongolia and the Angara-Ilim iron ore district in Eastern Siberia [Barenbaum, 2013c].

Plateau Dariganga. It is known that in Cenozoic powerful tectonic-magmatic processes took place in Central Asia. They generated a large number of basalt fields in the formation of which were attended by numerous volcanic centers, which quickly migrated and disappeared [Milashev, 1984]. Plateau Dariganga that arose at the Neogene-Quarter boundary, is one of such fields. Its area is about $20 \times 10^3 \text{ km}^2$. There are lots of volcanoes (~ 220) with diameters up 3-4 km. Plateau consists of four layer basalts total power up to 200 m with age of the Pliocene-Pleistocene. Basalts are alkaline and include deep-seated xenoliths. Under the terms of the crystallization of ultrabasites the depth of origin magmas estimated more of 100 km [Kaminsky, 1984].

Angara-Ilim district covers an area of $400 \times 600 \text{ km}^2$. The district refers to the Siberian trapean province, which has emerged at the Permian-Triassic boundary. In the area are revealed ~ 50 magnetite diatremes and same number structures with unexplored pipe structure, as well as about 10 volcanoes in the central zone. The diatreme pipes have a diameter of up to 2 km and are filled tuffs on many hundreds of meters. Under layer tuffs there are trapean agglomerates. Considered that agglomerates correspond to upper parts necks, which fill pipes below level of 1500-2000 m [Strakhov, 1978]

We believe that plateau Dariganga arisen in result of cometary bombardment of $5 \div 1$ million years ago, whereas diatremes of Angara-Ilim district arisen in bombardment of 250 million years ago, which was about 100 times more intense. The origin of the plateau we explain in that the quantity of a large comets impinging on its area was many more than near it. As a result lithosphere under plateau has

received significant heating that led to forming there large asthenospheric lens caused outpouring basalts and lifting surface. Surface plateau has been covered by system of cracks and diatremes, which became magma transporters for a large number of volcanoes.

The situation is different in Eastern Siberia. There maximum density of bombarding comets was on north of Siberian platform. Moreover, bombardment was so intensive and powerful that in during ~1 million years was produced volume of lava ~2 million km³ which occupies area ~4 million km². As known the greatest quantity of lava was poured out near Norilsk where thickness of trapean depositions reached ~1 km. In Angara-Ilim region located 1600 km south volcanism was weaker. Except center region the magma quantity in most diatremes was insufficient, so that top of pipes were filled tuffs. However, in center of arisen asthenospheric lens the magma is reached surface.

The situation is different in Eastern Siberia, where maximum of density bombarding comets has been on north of Siberian platform. Moreover, bombardment was so intensive and powerful that volume lava ~2 million km³ on area ~4 million km² has been created in during ~1 million years. As known, intensively of all lava poured out near Norilsk where thickness of trapean depositions reached ~1 km. In Angara-Ilim region located 1600 km south volcanism was weaker. Except center region the magma quantity in most diatremes was insufficient, so that top of pipes were filled tuffs. However, in center of arisen asthenospheric lens the magma is reached surface. In Angara-Ilim region located 1600 km south volcanism was weaker. Magma quantity in most diatremes of this region except its center part was insufficient, so that the top of diatremes turn out tuffs. However, in center of arisen asthenospheric lens where volcanoes exist the pipes were filled magma wholly.

Thus galactic comets are able create in lithosphere of planets large magma chambers, and in cases high intensity cometary fallings also very big asthenospheric lens which cause strong lifting of surface. These fundamental conclusions may be confirmed using Venus data.

Venus. Rocks of lithosphere Venus and Earth are very similar. Therefore, structures created galactic comets on Venus like the Earth. Let us briefly consider their similarities and differences.

Shield volcanoes. Volcanoes Venus are very similar to seamounts of our planet, but smaller. Most have a diameter of 1-20 km and a height of several hundred meters. Volcanoes number is ~ 10⁶ and distribution on sizes is exponentially [Aubele, Slynta, 1990]. Note that their number of the same order as Earth seamounts and craters on planets with no atmosphere. At that, shield volcanoes Venus are grouped into fields of ~60-300 km in diameter [Aubele et al., 1992], i.e. of same dimensions as diatreme fields on Earth [Milashev, 1984].

Craters. Venus found 880 large craters (Fig. 2). There are about as many as on Earth, but they are distributed according to an exponential law, which is not compatible with the assumption their education at falling asteroid bodies.

Coronae and Montes. Venus revealed 340 tectonic-magmatic uplifts rounded shapes called coronae and 115 canteens (plateaus) mountains – Montes [Wikipedia]. Distribution Coronae and Mons on sizes are shown in Fig.

3, and on latitude in Fig. 4. Distribution of Coronae and Montes (Fig. 3) excepting area of small diameters distorted by observation selection, obeys exponential dependence, which is sign of its cometary formation. This conclusion is confirmed by Fig. 4 where the densities of craters, Coronae and Montes on Venus are compared with similar distribution by latitude craters on Mars formed by asteroids and galactic comets. Unlike most of Martian craters, which have been formed during the last cometary shower the Coronae and Montes have much greater age. Coronae and Montes we consider as different stages of evolution of objects of one type, which are created cometary showers of very high density. At that, Montes arise first and later transform into Coronae.

Of course, these author's considerations about mechanism interaction of galactic comets with planets need further elaboration and justification.

References

1. Aubele J.C., Slynta E.N. (1990). Venus domes: characteristics and origin, Annu. Meet. Dallas. Texas. Abstr. with programs. V.22, № 04151/ Geological Society of America, c. A80.
2. Aubele J. C., J. W. Head, L. S. Crumpler et al. (1992) Fields of small volcanoes on Venus (shield fields): characteristics and implications, Lunar & Planet Sci., V.23, pt.1. pp. 47-48.
3. Cliffird T. H. (1966). Tectono-metallogenic units and metallogenic provinces of Africa, Earth Planet. Sci. Lett., V.1, №6, pp. 421-434.
4. Artyushkov E.V. (1994). Newest uplifts of terrestrial crust on continents as consequences lifting of great hot matter masses from mantle, Doklady Akad. Nauk, V.336, №5, pp. 680-683.
5. Barenbaum, A.A. (2002). Galaxy, Solar system, Earth. Subordinated processes and evolution. Moscow: GEOS, 393 p. (in Russian).
6. Barenbaum A.A. (2010). Galaxycentric paradigm in geology and astronomy, Moscow: LIBROKOM, 544 p. (in Russian).
7. Barenbaum A.A. (2011). Tectonic-magmatic processes in the oceans and continents as indicators fallings of galactic comets, Mater. Int. conf. commemorating V.E. Haina: The modern state of Earth Sciences, Moscow: Moscow State University. <http://khain2011.web.ru/> pp. 166-171.
8. Barenbaum A.A. (2012). On the origin recent uplifts the crust. New formulation of problems global geodynamics, Uralian Geological Journal, № 6 (90), pp. 3-26. (in Russian).
9. Barenbaum A.A. (2013). A possible mechanism of heating lithosphere rocks galactic comets, Uralian Geological Journal, № 1(91), pp. 21-39. (in Russian).
10. Barenbaum A.A. (2013a). The response lithosphere on fallings of galactic comets (I): the formation of volcanic-basaltic layer of the oceans crust, XIV Intern. conf.: Physical-chemical and petrological studies in geosciences, GEOKHI - IFZ - IEM - IGEM RAS, Moscow-Borok 7-10.10.2013, pp. 31-34. (in Russian).
11. Barenbaum A.A. (2013b). The response lithosphere on fallings of galactic comets (II): the origin of diamondiferous kimberlite pipes, Ibid. pp. 35-38. (in Russian).

12. Barenbaum A.A. (2013c). The response lithosphere on fallings of galactic comets (III): the intraplate magmatism and its manifestations, *Ibid.* pp. 39-42. (in Russian).
13. Barenbaum A.A. (2013d). About one of important tectonic-magmatic consequences fallings galactic comets into the Atlantic Ocean (Announcement 1), Proceedings of the XX International Scientific Conference on Marine Geology: Geology of Seas and Oceans. T.V. Moscow: GEOS. pp. 6-10.
14. Barenbaum A.A. (2013i). The space hypothesis of breaks formation in oceanic sedimentation (Report 2), *Ibid.* C.11-15. (in Russian).
15. Barenbaum A.A. (2013f). The young volcanism as evidence of recent uplifts Earth's crust in World Ocean (Report 3), *Ibid.* pp. 16-20. (in Russian).
16. Barenbaum, A. A., V.E. Hain, N.A. Yasamanov (2004). Large-scale tectonic cycle: an analysis from standpoint of galactic concept, *Vestnik MGU. Ser.4. Geology.* №3. pp. 3-16.
17. Barenbaum A. A., J. B. Gladenkov, N. A. Yasamanov (2002). The geochronological scale and astronomical time (modern condition of problem), *Stratigraphy. Geological correlation.* V.10. №2. pp. 3-14.
18. Barenbaum A.A., V.V. Shuvalov (2007). Modeling interactions of galactic comets with atmosphere, *Physics extreme states of matter-2007*, Ed. Fortov V.E. etc., Chernogolovka: IPCP RAS, pp. 139-140 (in Russian).
19. Blyuman B. A. (2011). The Earth crust of oceans based on materials of international programs deepwater drilling in the World Ocean. St. Petersburg: VSEGEI. 344 p.
20. Kazimirov D. A., B. D. Sitnikov, G.A. Poroshkova and others (1980). The density distribution of craters on the Moon, Mercury and Mars. Preprint GIN-GAISH (in Russian).
21. Kaminsky F. V. (1984). *Diamondiferous non-kimberlite igneous rocks*, Moscow: Nedra. 173 p.
22. Lavrentiev M. A. (1959). Problem of penetration at space velocities, *Artificial satellites Earth*. Moscow: Academy Sciences USSR, MY. 3, pp. 61-65. (in Russian).
23. Lavrentiev M.A., B.V. Shabat (1977). Problems of hydrodynamics and their mathematical models, *Nauka*. 408 p. (in Russian).
24. Milashev V. A. (1984). Pipes explosion, Leningrad: Nedra. 268 p. (in Russian).
25. Strahov L. G. (1978) Ore-bearing volcanic apparatus of southern Siberian platform. Novosibirsk: Nauka. 118 p. (in Russian).
26. Panayev V.A., S. P. Mitulov (1993). Seismic-stratigraphy sedimentary cover of the Atlantic Ocean, Moscow: Nedra. 247 p. (in Russian).
27. Wikipedia.org/wiki/ List of craters on Venus, List of coronae on Venus, List of montes on Venus.

Kadik¹ A.A., Koltashev V.V. ², Kryukova¹ E.B., Plotnichenko² V.G., Tsekhonya¹ T.I., Kononkova¹ N.N. Peculiarities of C–O–H volatile solubility in FeO–Na₂O–Al₂O₃–SiO₂ melts

equilibrated with liquid Fe alloy and graphite at 4 GPa and 1550°C

¹ V. I. Vernadsky Institute of Geochemistry and Analytical Chemistry RAS, Moscow

² Fiber Optics Research Center RAS, Moscow

Abstract. IR and Raman spectroscopy techniques are used to study the magmatic melts FeO–Na₂O–SiO₂–Al₂O₃ produced at a pressure of 4 GPa, temperature 1550 °C and oxygen fugacity values of $\Delta \log fO_2(IW) = -2 \div -5$ equilibrated with the metal Fe phase and graphite. Vibrational bands are attributed to the molecules and species formed during the experiments. The dependences of vibrational band intensities on oxygen fugacity and structural NBO/T parameter of glasses are presented.

Key words: COH volatiles, Raman and IR spectroscopy, iron, graphite, early Earth's mantle, hydroxyl, molecular H₂O.

Citation: Kadik A.A., V.V. Koltashev, E.B. Kryukova, V.G. Plotnichenko, T.I. Tsekhonya, N.N. Kononkova (2014). Peculiarities of C–O–H volatile solubility in FeO–Na₂O–Al₂O₃–SiO₂ melts equilibrated with liquid Fe alloy and graphite at 4 GPa and 1550°C. *Experimental geochemistry.* V. 2. No.

To elucidate the features of carbon and hydrogen solubility in iron-bearing magmatic melts equilibrated with metal Fe phase and graphite at oxygen fugacity values (fO_2) by 2-5 orders of magnitude below the buffer equilibrium iron-wüstite $\Delta \log fO_2(IW)$, the experiments are carried out with the melts of FeO–Na₂O–SiO₂–Al₂O₃ composition at high pressure 4 GPa and temperature 1550°C.

Studies by the methods of IR and Raman spectroscopy of silicate glasses produced as a result of high-temperature and high-pressure experiments (Figs. 1 and 2 accordingly) testify to a formation in them of C–H bonds in the form of CH₄ molecules and groups CH₃[–] (Si–O–CH₃). In oxidized form carbon is present in the melt as CO₂ molecule and carbonate CO₃^{2–} ion, but judging by the absorption band intensity in the IR spectra their concentration is rather low. Besides the species with carbon, the dissolved hydrogen is present in the melt in the form of molecules H₂, H₂O and hydroxyl groups OH[–]. Contrary to [Wetzel et al. 2013], IR spectroscopy of glasses doesn't reveal any absorption band at 2110 cm^{–1} which could point to a formation of Fe(CO₅) complex in the melts. Probably its absence is caused by too low oxygen fugacity (fO_2) values in our experiments. At the same time, IR and Raman spectra testify that carbon is dissolved in the form of species with double bonds C=O. Their formation in the melts at low fO_2 values was established for the first time in [Kadik et al. 2010; 2013].

Figure 3 shows changes in the IR and Raman spectra of silicate melts, characterizing the influence of fO_2 and structural parameter (NBO/T) of glasses on the content of groups and molecules (OH[–] + H₂O), H₂O, CH₄, H₂ and species with double bond C=O. They are given in the form of Abs/Abs^o and I/I^o ratios, where Abs^o and I^o are the values of absorption coefficient in the IR bands and integral Raman band intensity in the Raman bands for $\Delta \log fO_2(IW) = -1.8$. (a) – Values $Abs_{3548} / Abs_{3548}^o (I)$ and $Abs_{1632} / Abs_{1632}^o (2)$ for the IR bands at 3548 cm^{–1} and 1632 cm^{–1} in the field of (OH[–] + H₂O) and H₂O vibrations, accordingly. (b) – Values $I_{2915} / I_{2915}^o (I)$ and $I_{4130} / I_{4130}^o (2)$ for the Raman bands at 2915 cm^{–1} and 4130 cm^{–1} in the field of CH₄ and H₂ vibrations. (c) – Values $Abs_{1780} / Abs_{1780}^o (I)$ and $Abs_{1740} / Abs_{1740}^o (2)$ for the IR bands at 1780 cm^{–1} and 1740 cm^{–1} in the field of C=O double bond vibrations.

It is seen (Fig. 3) that with lowering fO_2 the concentrations of H_2O , OH^- and to some extent of H_2 decrease at a simultaneous considerable increase in CH_4 content. Concentration of species with $C=O$ bond sharply increases with lowering fO_2 and reaches its maximum value at $\Delta \log fO_2(IW) = -3$.

According to IR spectra, the total water content in glasses ($OH^- + H_2O$) has made 1.2–5.8 wt. % and also decreases with lowering fO_2 . High H_2O concentrations are

substantially determined by oxygen release at FeO reducing from the melt. Total carbon content at high H_2O concentrations (4.9–5.8 wt. %) has made about 0.4 wt. %. The NBO/T values were calculated with the account of total H_2O content in silicate glasses agree well with the IR spectroscopy data and have made in various experiments 0.80 (0.58), 0.63 (0.52), 0.32 (0.20) and 0.07 (0.04). In brackets the NBO/T values are indicated without the account of H_2O content in glasses.

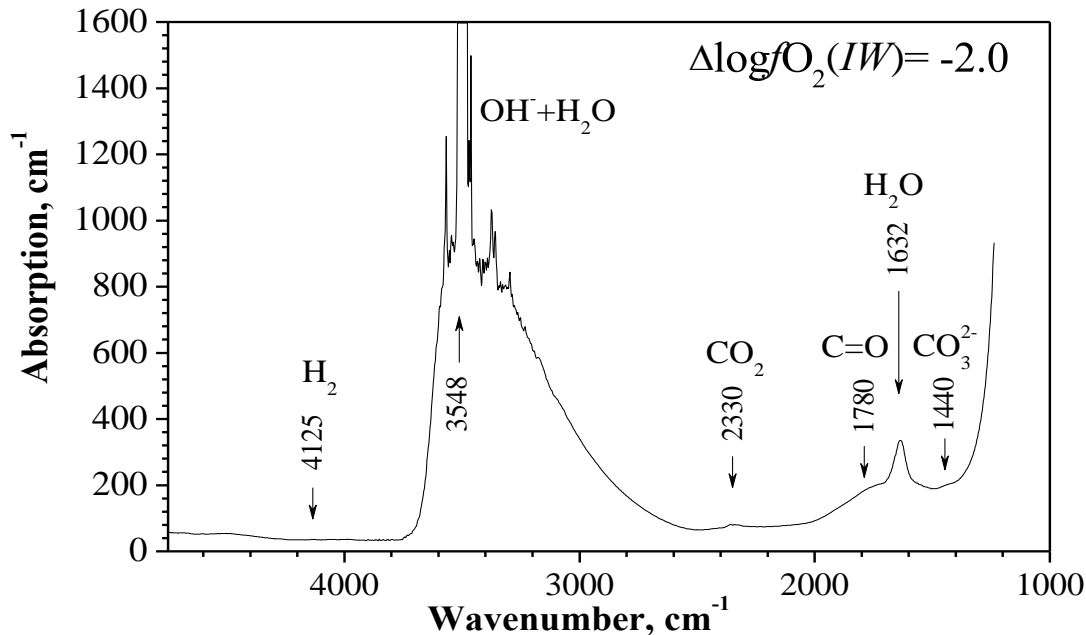


Fig. 1. IR spectrum of C–O–H-bearing aluminosilicate glass in the field of 5000–1000 cm^{-1} : $\Delta \log fO_2(IW) = -2.0$ (sample 846, $h = 70 \pm 3 \mu m$), where h is the thickness of a plane-parallel plate.

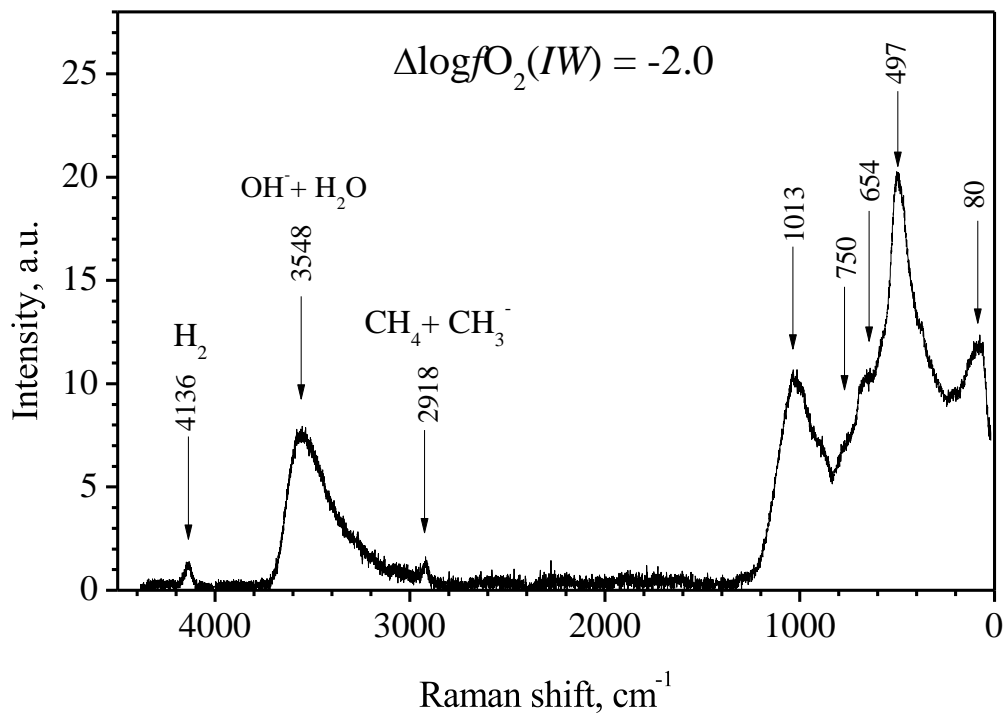


Fig. 2. Raman spectrum of C–O–H-bearing aluminosilicate glass in the field of 4500–1000 cm^{-1} : $\Delta \log fO_2(IW) = -2.0$ (sample 846).

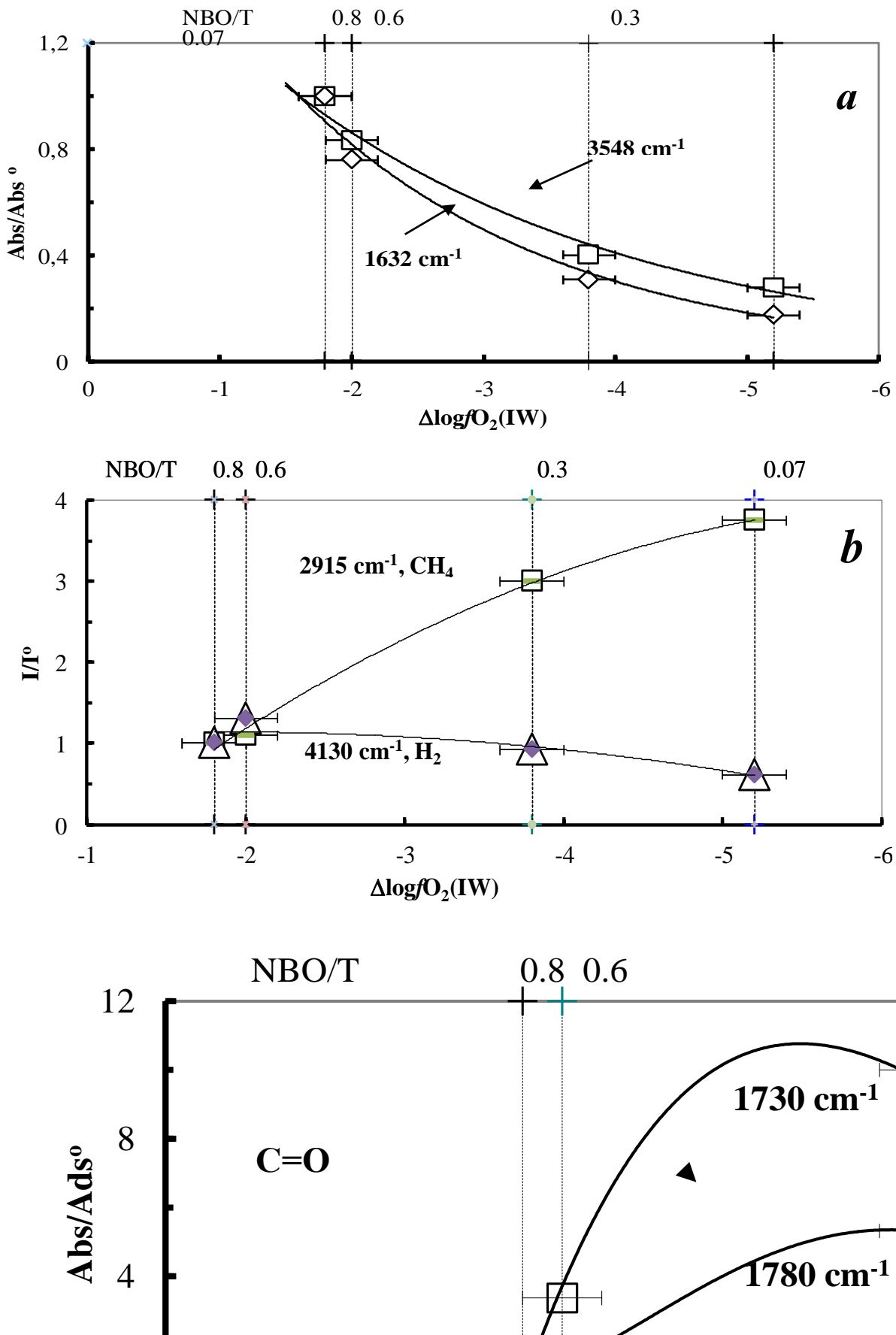


Fig. 3. Variation of absorption coefficient Abs/Abs_0 and integral intensity I/I_0 in IR and Raman bands: *a* – hydroxyl groups and molecules ($OH^- + H_2O$) and H_2O , *b* – molecules CH_4 and H_2 , *c* – species with double bond $C=O$ as a function of $\Delta \log fO_2(IW)$ and structural parameter (NBO/T) in silicate melts, where Abs_0 and I_0 are the parameter values at $\Delta \log fO_2(IW) = -1.8$.

In many respects the solution mechanisms of C–H species in silicate melts remain a discussion subject. The notions about them are summarized in [Mysen, 2012]. It is supposed that the main solution mechanism of C–H species in the melts is

$$\text{Si-O-Si (melt)} + \text{CH}_4 = \text{Si-O-CH}_3 \text{ (melt)} + \text{Si-O-H (melt)}$$

where Si–O–Si refers to bridging oxygen, and in Si–O–CH₃ and Si–O–H the oxygen bonds are non-bridging ones.

It is supposed that CH₄ molecules are sited in structural voids of silicate fluids similarly to the solution of rare gases [Carrol and Webster, 1994; Mysen and Richet, 2005] Apparently, this results in CH₄ solubility growth with NBO/T decreasing, i.e. with lowering the polymerization degree of the melts at constant temperature, pressure and *f*O₂ [Mysen et al., 2011; Dasgupta et al., 2013].

This work was made possible through support of Prog. No 28 RAS, RFBR grant No 14-05-00136a, ESD RAS project No9.

References:

1. Carrol M. R., J. D. Webster (1994). Solubilities of sulfur, noble gases, nitrogen, chlorine, and fluorine in magmas, in: Volatiles in magmas, Reviews in mineralogy, v. 30, p. 231–279, Min. Soc. Am., Washington D.C.
2. Dasgupta R., H. Chi, N. Shimizu, A. S. Buono, D. Walker (2013). Carbon solution and partitioning between metallic and silicate melts in a shallow magma ocean: implications for the origin and distribution of terrestrial carbon. *Geochim. Cosmochim. Acta*, v. 102, p. 191–212.
3. Hirschmann M. M., A.C. Withers (2008). Ventilation of CO₂ from a reduced mantle and consequences for the early martian greenhouse. *Earth and Planet. Sci. Lett.* No. 270, p. 147–155.
4. Kadik A. A., N. A. Kurovskaya, Yu. A. Ignat'ev, N. N. Kononkova, V. V. Koltashev, V. G. Plotnichenko (2010). Influence of Oxygen Fugacity on the Solubility of Carbon and Hydrogen in FeO–Na₂O–SiO₂–Al₂O₃ Melts in Equilibrium with Liquid Iron at 1.5 GPa and 1400°C. *Geochemistry International*, v. 48, No. 10, p. 953–960.
5. Kadik A. A., Yu.A. Litvin, V.V. Koltashev, E.B. Kryukova, V.G. Plotnichenko, T.I. Tsekhonya, N.N. Kononkova (2013). Solution behavior of reduced N–H–O volatiles in FeO–Na₂O–SiO₂–Al₂O₃ melt equilibrated with molten Fe alloy at high pressure and temperature. *Phys. Earth Planet. Inter.*, v. 214, p. 14–24.
6. Mysen B. O. (2012). Silicate-COH melt and fluid structure, their physicochemical properties, and partitioning of nominally refractory oxides between melts and fluids. *Lithos*, v. 148, p. 228–246.
7. Mysen B. O., K. Kumamoto, G.D. Cody, M.L. Fogel (2011). Solubility and solution mechanisms of C–O–H volatiles in silicate melt with variable redox conditions and melt composition at upper mantle temperatures and pressures. *Geochim. Cosmochim. Acta*, v. 75, p. 6183–6199.
8. Mysen B. O., P. Richet (2005). Silicate Glasses and Melts: Properties and Structure. In: *Developments in Geochemistry*, v. 10, ch.16, p. 560, Elsevier.

9. Wetzel D. T., S.D. Jacobsen, M.J. Rutherford, E.H. Hauri, A.E. Saal (2013). Degassing of reduced carbon from planetary basalts. *Proc. Natl. Acad. Sci.* <http://dx.doi.org/10.1073/pnas.1219266110>.

Kadik¹ A.A., Koltashev²V.V., Kryukova¹E.B., Plotnichenko² V.G., Tsekhonya¹T.I., Kononkova¹ N.N. Carbon and silicon solubility in liquid Fe–Si–C alloy equilibrated with FeO–Na₂O–SiO₂–Al₂O₃ melt

¹ Vernadsky Institute of Geochemistry and Analytical Chemistry, RAS, Moscow

² Fiber Optics Research Center, RAS, Moscow

Abstract. The melts FeO–Na₂O–SiO₂–Al₂O₃ produced at pressure 4 GPa, temperature 1550 °C and oxygen fugacity values Δlog*f*O₂ (*IW*) = -2 ÷ -5 and equilibrated with liquid Fe–Si–C alloy during the formation of magmatic ocean are investigated. Estimates of C and Si solution in the given melts are performed. It is shown that concentration of C in iron alloy globules depends on silicon content in it and, accordingly, on *f*O₂. It is reasonable to assume that during melting of the early reduced Earth's mantle at *f*O₂ values 4–5 log units below iron–wüstite (*IW*) buffer equilibrium *f*O₂(*IW*) the role of segregation of Fe alloys in carbon extraction from the reduced magmas into the forming planetary core will be less considerable, than it should be expected for higher *f*O₂ values.

Key words: experiment, magma ocean, metal core, oxygen fugacity, C and Si solubility.

Citation: Kadik A.A., V.V. Koltashev, E.B. Kryukova, V.G. Plotnichenko, T.I. Tsekhonya, N.N. Kononkova (2014).

Carbon and silicon solubility in liquid Fe–Si–C alloy equilibrated with FeO–Na₂O–SiO₂–Al₂O₃ melt. *Experimental geochemistry*. V. 2. No.

Paper is devoted to the experimental study of the behavior of carbon, hydrogen and oxygen volatiles during the Earth's differentiation that is closely related to the ways and mechanisms of the Earth's degassing, as well as to a composition and quantity of volatile components which were maintained in the mantle after the formation of the metal Earth's core [e.g., *Javoy, 1997; Cartigny et al., 2001; Marty, 2012*].

Experimental studies of FeO–Na₂O–SiO₂–Al₂O₃ aluminosilicate system equilibrated with liquid Fe–Si–C alloy and graphite at 4 GPa, 1550°C and oxygen fugacity values *f*O₂ 2–5 log units below iron–wüstite buffer equilibrium *f*O₂(*IW*) are carried out to estimate the C and Si solubility in Fe alloy during the magma ocean formation. In experiments *f*O₂ values correspond to existing notions about the conditions of the early chemical Earth's differentiation during melting and segregation of the metal Fe phase.

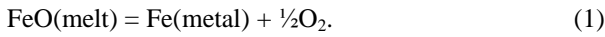
The experiments were performed in an anvil-with-hole apparatus of a large useful volume (6 cm³) at 4 GPa and 1550 °C [Litvin, 1979; 1991] under controlled hydrogen fugacity [Kadik, etc., 2004].

The starting material for experiments (Table 1) represented a finely dispersed mixture of albite glass (NaAlSi₃O₈, 80 wt. %) and FeO (20 wt. %), both pure and with addition of 2, 5 and 10 wt. % of silicon carbide powder (SiC), to provide low *f*O₂ values in experiments due to the reaction of oxidizing SiC at its interaction with iron-bearing silicate melt and hydrogen.

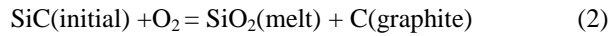
Abstracts

To saturate the investigated system with free carbon a high-pressure fusion was carried out in the presence of graphite disk.

The oxygen fugacity imposed on the experimental sample was controlled by redox reaction between hydrogen buffered externally and components of the Fe-bearing melt that was reduced with oxygen liberation and metal Fe phase



The initial silicon carbide (SiC) was unstable under the experimental conditions and completely consumed due to the oxidation reaction



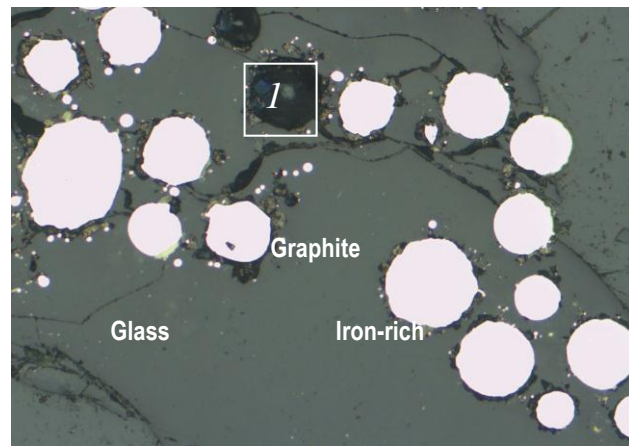
with a subsequent participation of carbon in the reactions with silicate melt components and hydrogen.

Table 1. Initial mixtures NaAlSi₃O₈ + FeO + SiC used in experiments (wt. %)

Initial mixture	Run	SiO ₂	Al ₂ O ₃	FeO	Na ₂ O	Si	C	Total
AbFeO+ 0 SiC	847	54.98	15.56	20	9.46	0	0	100
98AbFeO+2SiC	846	53.88	15.25	19.6	9.27	1.4	0.60	100
95AbFeO+5SiC	848	52.23	14.78	19	8.99	3.5	1.50	100
90AbFeO+10SiC	849	49.48	14.02	18.00	8.51	7.01	2.99	100

Note: AbFeO is the mixture of albite glass (NaAlSi₃O₈, 80 wt. %) and FeO (20 wt. %)

Fig. 1. Glass with droplets of metal Fe and graphite crystals in quenching sample products after the experiment at 4 GPa, 1550°C, $\Delta \lg f_{\text{O}_2}(\text{IW}) = -3.8$ (back-scattered electron image).



Calculation of oxygen fugacity was carried out from Fe and FeO content of the metal and silicate phases according to the equation $\Delta \lg f_{\text{O}_2}(\text{IW}) = 2 \lg(a_{\text{FeO}}/a_{\text{Fe}})$ [Drake *et al.*, 1989], and also on the basis of an empirical expression $\lg f_{\text{O}_2} = 2 \lg(X_{\text{FeO}}/a_{\text{Fe}}) - h/T(\text{K}) - \sum d(X_i)$, as a function temperature and composition [Ariskin *et al.*, 1993].

As a result of performed experiments the system presented by three-phase equilibrium is produced: iron alloy + silicate melt + graphite (Fig. 1). Distribution of FeO, Na₂O, Al₂O₃, SiO₂ components in glass and of carbon in glass and iron alloy globules has appeared to be rather homogeneous (Table 2) that testifies to achievement of chemical equilibrium during the experiments.

As a result of reaction of silicon carbide with silicate melt and O₂ at FeO reduction, f_{O_2} values inside the

platinum ampoule appear to be considerably below $f_{\text{O}_2}(\text{IW})$. Thus the decrease of f_{O_2} values is in direct ratio to SiC quantity in initial mixture.

The chemical composition of glasses is characterized by a considerable reduction of FeO content with lowering f_{O_2} values in the experiments (Table 2) that reflects the process of FeO reduction in the melt with a formation of liquid Fe phase due to the reaction Eg.(1).

Table 2. The chemical composition of glasses and iron-rich globules after the experiments at 4 GPa and 1550 °C determined by electron microprobe (wt. %)

	$\Delta \lg f_{\text{O}_2}(\text{Parameter})$			SiO ₂	Al ₂ O ₃	FeO	Na ₂ O	WO ₃	Total
	Run	IW)							
Glass	847	-1.8	average of 10	58.44	16.64	12.49	10.31	0.19	98.07
			δ	0.38	0.16	0.15	0.35	0.11	0.41
	846	-2.0	average of 10	60.08	17.18	10.7	10.26	0.18	97.77
			δ	0.5	0.19	0.2	0.53	0.06	0.33
	848-1	-3.4	average of 9	70.51	17.57	1.88	11.05	0.20	101.21
			δ	0.50	0.17	0.31	0.30	0.05	0.25
	848-2	-3.8	average of 9	68.67	17.47	1.39	11.02	0.17	98.67
			δ	0.47	0.17	0.06	0.16	0.06	0.25
	849	-4.0	average of 9	71.51	17.35	1.14	10.49	0.04	100.16
			δ	0.57	0.17	0.29	0.23	0.02	0.25
849n	-5.2	average of 9	71.91	18.09	0.24	9.77	0.09	100.01	
		δ	0.26	0.12	0.16	0.13	0.02	0.21	

Run	$\Delta \lg fO_2(IW)$	Parameter	Fe	W	Si	Total
847	-1.8	average of 9	92.87	3.24	0.03	96.14
		δ	0.50	0.35	0.01	0.56
846	-2.0	average of 4	95.48	1.69	0.09	97.26
		δ	1.51	0.44	0.01	1.05
848-1	-3.4	average of 9	96.58	0.21	0.03	98.82
		δ	0.30	0.12	0.01	0.26
848-2	-3.8	average of 9	96.36	0.21	0.03	96.60
		δ	0.31	0.07	0.02	0.30
849	-4.0	average of 9	96.19	0.19	0.03	96.41
		δ	0.57	0.09	0.03	0.41
849n	-5.2	average of 8	85.37	0.24	13.27	98.88
		δ	0.73	0.08	1.17	0.74

Figure 1 shows the quantities of Fe and O vs fO_2 which were released during the experiments according to two processes, namely: (1) FeO reducing with formation of metal Fe phase and O_2 ; (2) SiC oxidizing in initial mixture with SiO_2 and C formation in the melts. Amount of oxygen wasted for oxidizing SiC due to the reaction (2) is determined by Si content in initial mixture used in the experiments. The total amount of oxygen released at FeO reducing by the reaction (1) has appeared to be above the values necessary for oxidizing Si according to the reaction (2) (curves 2 and 3 in Fig. 1). It is reasonable to assume that the redundant oxygen was consumed for the formation of C–O–H species in silicate liquid, in particular such as H–O and C–O. Some amount of oxygen could be dissolved in liquid Fe alloy. The last suggestion is confirmed by concentration of oxygen in globules of iron alloys which has made about 0.6–0.8 wt. %.

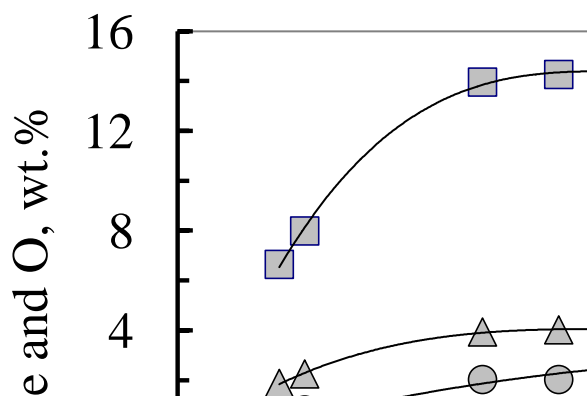


Fig. 2. Quantities of metal Fe phase and oxygen (wt. %) vs fO_2 produced during the experiments: 1, Fe quantity and 2, O quantity when FeO is reduced from the melt $FeO-Na_2O-SiO_2-Al_2O_3$ due to the reaction (1) $FeO(melt) = Fe(metal) + \frac{1}{2}O_2$; 3, O quantity consumed in SiC oxidation from initial mixture with SiO_2 formation in the melts due to the reaction (2) $SiC(initial) + O_2 = SiO_2(melt) + C(graphite)$.

Determinations of carbon content in glasses using electron microprobe are close in the whole to CHN-metry data at $\Delta \lg fO_2(IW) = -1.8 \div -2.0$ and testify to a reduction of the total C content with lowering fO_2 (Fig. 2). According to ion microprobe and CHN-metry data the total H content has made 0.1–0.4 wt. %, also decreasing with lowering fO_2 (Fig. 2). Carbon content in liquid Fe alloys depended on concentration of silicon and, apparently, oxygen solubility, lying within 0.3–3.65 wt. %. Low carbon concentrations (~0.2 wt. %) are apparently related to an essential growth of Si content in liquid Fe

alloy, which has made about 13 wt. % at fO_2 values 4–5 log units below $fO_2(IW)$.

It is shown that C concentration in globules of Fe alloy depends on Si content in it and, accordingly, on fO_2 . At fugacity values $\Delta \lg fO_2(IW) = -2.0$ and -3.8 and low Si concentrations (0.1–0.3 wt. %) it makes 3.7 ± 0.2 and 2.7 ± 0.2 wt. %, accordingly. At $\Delta \lg fO_2(IW) = -5.2$ Si concentration in Fe–Si–C alloy reaches 13.3 wt. % with simultaneous reduction of C concentration to 0.3 wt. %. Similar influence of Si on carbon solubility in liquid Fe is well-known from thermodynamics of metal alloys [e.g., Bouchard and Bale, 1995]. It was confirmed in experiments at high pressures and temperatures [e.g., Gessman et al., 2001; Ricolleau et al., 2011], showing that with decrease in fO_2 and increase in siderophile Si properties the graphite solubility in liquid Fe decreases (Fig. 2). According to microprobe analysis data the Fe alloy contained about 0.6–0.8 wt. % of dissolved oxygen. It also could lead to a decrease of carbon solubility in liquid Fe alloy. Thus, it is reasonable to assume that during melting of the early reduced Earth's mantle at fO_2 values 4–5 log units below iron–wüstite (IW) buffer equilibrium $fO_2(IW)$ the role of segregation of Fe alloys in carbon extraction from the reduced magmas into the forming planetary core will be less considerable, than it should be expected for higher fO_2 values.

This work was made possible through support of Prog. No 28 RAS, RFBR grant No 14-05-00136a, ESD RAS project No 9.

References

1. Ariskin, A.A., Borisov, A.A., Barmina, G.S., 1993. Simulating iron-silicate melt equilibrium in basaltic systems. *Geochem. Inter.* 30, 13–22.
2. Bouchard D. and Bale C.W., 1995. Simultaneous optimization of thermodynamical data for liquid iron alloys containing C, N, Ti, Si, Mn, Si, and P. *Metall. Trans. B*, 26B, 467–483.
3. Cartigny P., Jendrzejewski F., Pineau F., Petit E., Javoy M., 2001. Volatile (C, N, Ar) variability in MORB and the respective roles of mantle source heterogeneity and degassing: the case of the Southwest Indian Ridge. *Earth Planet. Sci. Lett.*, 194, 241–257.
4. Drake, M.J., Newsom, H.E., Capobianco, C.J., 1989. V, Cr, and Mn in the Earth, Moon, EPB, and SPB and the origin of the Moon: Experimental studies. *Geochim. Cosmochim. Acta* 53, 2101–2111.

5. Gessman C.K., Wood B.J., Rubie D.C., and Kilburn M.R., 2001. Solubility of silicon in liquid metal at high pressure: implications for the composition of the Earth's core. *Earth Planet Sci. Lett.*, 184, 367-376.
6. Javoy, M., 1997. The major volatile elements of the Earth: their origin, behavior, and fate. *Geophys. Res. Lett.* 24, 177–180.
7. Kadik A.A., Pineau F., Litvin Y.A., Jendrzewski N., Martinez I., Javoy M., 2004. Formation of carbon and hydrogen species in magmas at low oxygen fugacity during fluid-absent melting of carbon-bearing mantle. *Jour.Petrol.*, 45 (7), 1297–1310.
8. LitvinYu.A., 1979. Distribution of pressure up to 40 Kbar and temperature up to 1500oC in the solid-state cell of large useful volume. *Priboiy i Tekhnika Experimenta (Instruments and Technics for Experiment)*, № 5, 207–209 (in Russian).
9. LitvinYu.A., 1991. *Physico-Chemical Study of Melting Relations of the Deep-Seated Earth's Substance*: Moscow, Publishing House “Nauka”, 312 p. (in Russian)
10. Marty B., 2012. The origins and concentrations of water, carbon, nitrogen and noble gases on Earth. *Earth Planet. Sci. Lett.*, 313–314, 56–66.
11. Ricolleau A., Fei Y., Corgne A., Julien S., James Badro J., 2011. Oxygen and silicon contents of Earth's core from high pressure metal–silicate partitioning experiments. *Earth Planet Sci. Lett.*, 310, 409–421.

Lavrentjeva Z. A. , Lyul A.Yu. The trace element studies of grain-sized fractions from light and dark lithologies Pesyanoe aubrite

V. I. Vernadsky Institute of Geochemistry and Analytical Chemistry RAS, Moscow

Abstract. The results of trace element abundances in separated grain-sized fractions from Pesyanoe aubrite are reported. From observed differences of compositions of grain-sized fractions from Pesyanoe it follows that our trace element data accord with this idea that aubrites reflect melting processes within or on the surface on the parent body. All of these data, together with results from previous studies, indicate that aubrite are igneous rocks, brecciated, that are thought formed by to melting, fractionation, and differentiation of enstatite chondrite-like precursor lithologies.

Key words: aubrite, elemental abundance.

Citation: Lavrentjeva Z.A., A.Yu. Lyul (2014). The trace element studies of grain-sized fractions from light and dark lithologies Pesyanoe aubrite. *Experimental geochemistry*. V. 2. No.

Introduction. Aubrites, or enstatite achondrites, are differentiated reduced meteorites, most of them fragmental or regolith breccias. They consist mainly of Fe-free orthopyroxene (on average 90%, e.g. [Reid and Cohen, 1967; Watters and Prinz, 1979; Keil, 2010]), with plagioclase, diopside, forsteritic olivine, Fe-Ni metal, and sulfides as minor modal components [Watters and Prinz, 1979]. Their formation under very reducing conditions, similar to those experienced by enstatite chondrites, is reflected by incorporation into sulfide of nominally lithophile elements (Cr, Ti, Mn, Mg, Ca) as trace elements [e.g. Watters and Prinz, 1979] or as major elements with the formation of minerals such as oldhamite (CaS), alabandite (MnS) and daubreelite (FeCr₂S₄), among others. The origin of aubrites containing many unique for

planetary materials minerals and their genetic relationship to enstatite chondrites are controversial so far. The aubrite are igneous rocks, many brecciated that are thought to have been formed by the melting, fractionation and differentiation of enstatite chondrite-like precursor lithologies, as is likely in view of the compositional and isotopic similarities of aubrites and enstatite chondrites. While of the 27 aubrites, 15 are fragmental breccias, 6 are regolith breccias, and 6 are described as nonbrecciated, their ingredients are clearly of igneous origin and formed by melting and fractional crystallization possibly of a magma ocean. This is indicated by the occurrence of variety of lithic clasts of igneous origin, and by the REE and other element distributions [Keil, 2010]. Rare earth element (REE) patterns (in particular Eu anomalies) have been interpreted as suggestive of an igneous origin (5, 7). Whole-rock REE patterns, with negative Eu anomalies have been used as one of the major arguments in favor of an igneous origin for aubrites (2, 5). A variety of restrictions and specifications on aubrite formation processes were received from trace element data for the Pena Blanca Spring mineral separates [Lodders et al., 1993]. To receive more information about of aubrite chemistry the trace elemental composition of the separate fractions from Pesyanoe aubrite was determined by INAA.

Samples and method. The Pesyanoe aubrite (fell 1933, Russia) is gas-rich polymict regolith breccia [Lorenzetti et al., 2003] consisting of several pyroxenic lithologies, clastic and melt breccias, melt rocks, glass spherules and exotic chondrite inclusions [Lorenz et al., 2005]. Among the aubrites, Pesyanoe is one of a small number containing abundant solar-type noble gases [Lorenzetti et al., 2003], testifying to its origin as a regolith breccia. Watters and Prinz [Watters and Prinz, 1979] reported a mineral assemblage of enstatite (Fs_{0.1}), forsterite (Fa_{0.1}), diopside (Fs_{0.1} Wo_{43.6}), plagioclase (Ab_{93.6}), Ti-bearing troilite (0.46 wt% Ti), oldhamite, daubreelite, alabandite, FeNi metal (0.29 wt% Si) and schreibersite. Pesyanoe is a typical aubrite, containing of an assemblage of highly reduced minerals.

In the present paper the results of trace element abundances in separated grain-sized fractions, from Pesyanoe aubrite are reported. The fractions were selected by particle-size analysis. The element composition of fractions was analyzed at the Central Laboratory of GEOKHI RAS using optimized version of neutron-activation analyses developed for analyzing extraterrestrial material [Kolesov et al., 2001].

Results and discussion. “Fine-grained” fractions (“matrix”, 1<d<45 μm) (Fig.1). The fine-grained fractions are enriched in lithophilic by factors Na (1.2-1.5xCI); Ca (1.1–1.9xCI); Sc (1.6–1.7xCI) and are depleted in siderophilic Ni, Co, Fe, Au, Ir (0.002-0.2xCI) elements. REE analyses of fractions showed that they have high REE concentrations with a light (1.0–2.7xCI) and heavy (1.5–3.3xCI) rare earth elements (LREE and HREE) enriched and with both positive and negative (Fig.1) Eu-anomalies. The enrichment a fine-grained fractions in many elements with different geochemical properties, including REE also, suggest that one contain various accessory minerals (oldhamite and plagioclase) – the host minerals for many trace elements. For track investigation [Kasharov et al., 2002] it was taken a “matrix” sample of the Pesyanoe aubrite. Obtained nuclear-track, TL data

show that the initial Pesyanoe meteorite constrain material was contained the compounds of the essentially different radiation and shock-thermal pre-history. There are a high probability that the fossil track characteristics of Pesyanoe individual enstatite grains refer to their history of a radiation, thermal and shock-thermal influence chiefly occurred on pre-accretion and/or regolith stages of a parent body formation of this aubrite. The possible “pure thermal” metamorphism inside a parent body, would result about the same manner in all enstatite grains. But guide essential difference of TL-parameters, measured for the several “matrix” samples, indicate on very small influence of this process in comparison with the more effective and heterogeneous shock-thermal process during of exogenous reworking of this meteorite material. Absence of the visual variation of concentration of some volatile-refractory elements in a number the “matrix” samples of different

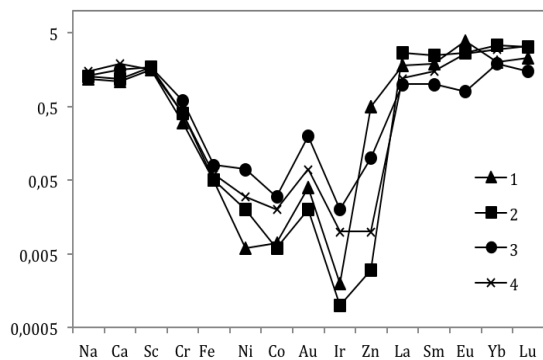
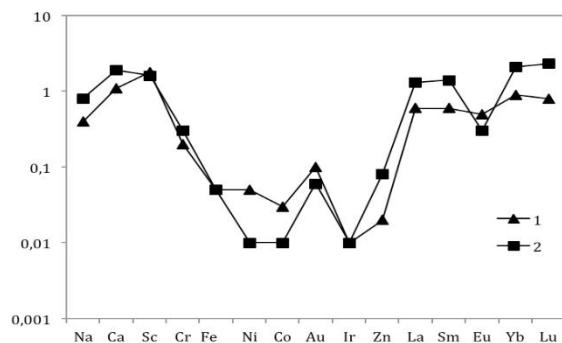


Fig 1. CI – normalized trace element abundance patterns of “fine-grained” fractions. 1 – light and 2 – dark lithologies of “matrix”; 3 – light and 4 -dark lithologies of 1<d<45 μm fractions.

“Coarse-grained” fractions (100<d<160 μm) (Fig.3).

The coarse-grained fractions are depleted in Na (0.4-0.8xCI) versus (1.2–1.5xCI) in fine-grained fractions and are depleted in siderophilic Ni, Co, Fe, Au, Ir (0.01-0.1xCI) elements. The refractory siderophile element Ir (0.001–0.02xCI) are distinctly more depleted in all fractions than “normal” siderophiles Ni (0.006–0.07 x CI) and Au (0.01–0.2 x CI). A similar trend is show by eucrites [Morgan et al., 1979] as well as lunar dunite, mare



sizes correlate with the low-level shock-thermal reworking of material consisting investigated aubrite in their metamorphic history. The aubrite Pesyanoe matter during geology history, starting from the early irradiation in the regolith or more early environment conditions, do not underwent to influence of the shock-thermal events stronger than P≥20 Gpa and T≥500K during of the short-time interval.

“Mean-grained” fractions (45<d<71μm; 71<d<100 μm) (Fig.2)

Na abundances of dark (1.0-1.2xCI) are higher than of light (0.7–0.9xCI) lithologies. Fractions are enriched in Sc (1.5–1.8) and are depleted in siderophilic Ni, Co, Fe, Au, Ir (0.002–0.08xCI) elements. The REE patterns have HREE enrichment relative LREE and CI chondrites with positive Eu and positive Yb and negative Eu-anomalies.

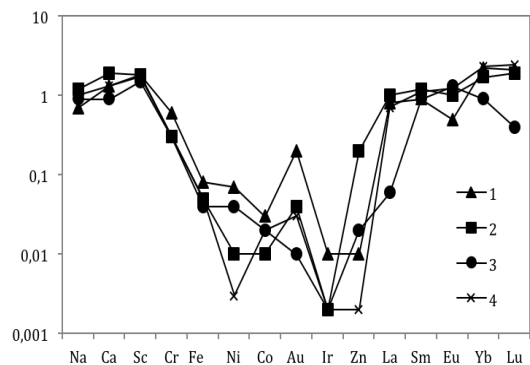


Fig 2. CI – normalized trace element abundance patterns of “mean-grained” fractions. 1 – light and 2 – dark lithologies 45<d<71 μm fractions; 3 – light and 4 – dark lithologies of 71<d<100 μm fractions.

basalts, and pristine highland rock [Wolf et al., 1979; Wolf and Anders, 1980]. This trend parallels the nobility of the metals, and therefore has been attributed to equilibrium distribution between metal and silicate, less noble metals being less completely extracted from silicate. Inasmuch as the Pesyanoe aubrite also shows this trend, it appears that the aubrite pattern is at least consistent with an igneous origin. The REE patterns have HREE enrichment – $(Lu/La)_{\text{fractions 1, 2}} / (Lu/La)_{\text{CI}}$.

Fig 3. CI – normalized trace element abundance patterns of “coarse-grained” abundance patterns of “coarse-grained” abundance patterns of “coarse-grained” fractions. 1 – light and 2 – dark lithologies of 100<d<160 μm fractions.

On the basis of the data presented here, the accessory minerals (oldhamite and plagioclase) are the major REE carrier in the aubrites. Plagioclase is the only mineral measured with a positive Eu anomaly and LREE enrichment [Wheelock et al., 1990]. All other phases have negative Eu anomalies and diopside, alabandite, and some oldhamite have HREE enrichment trends. Oldhamite is the

major REE carrier in the aubrites. Olhamites, have REE signatures consistent with partial melting and melt extraction in the aubrite parent body as well as remnant from nebular condensation. [Floss et al, 1990; Floss and Crozaz, 1993]. An igneous origin is further supported by Eu anomalies in plagioclase and “magmatic” mineral fractions [Graham and Henderson, 1985].

Conclusion. From observed differences of compositions of grain-sized fractions from Pesyanoe it follows that our trace element data reflect processes on the surface on the parent body, it is possible and melting processes. All of these data, together with results from previous studies, indicate that aubrites are igneous rocks, brecciated, that are thought formed by to melting, fractionation, and differentiation of enstatite chondrite-like precursor lithologies.

References

1. Reid A. M., Cohen A. J. (1967). Some characteristics of enstatite from enstatite achondrites. *Geochim. Cosmochim. Acta*, v. 31, p. 661-672.
2. Watters T. R., Prinz M. A. (1979). Aubrites: Their origin and relationship to enstatite chondrites. *Proc. Lunar Planet. Sci. Conf. 10th*, 1, p. 1073-1093.
3. Keil K. (2010). Enstatite achondrite meteorites (aubrites) and the histories of their asteroidal parent bodies. *Chem. Der Erde*, v. 70, p. 295 – 317.
4. Wolf R., Ebihara M., Richter C.R., Anders E. (1983). Aubrites and diogenites: trace elements – clues to their origin. *Geochim. Cosmochim. Acta*, v. 47, p. 2257-2270.
5. Lorenzetti S., Eugster O., Busemann H., Marti K., Burbine T. H., McCoy T. (2003). History and origin of aubrites. *Geochim. Cosmochim. Acta* v. 67, p. 557-571.
6. Lorenz C., Ivanova M.A., Kurat G., Brandstaetter F. (2005). FeO-rich xenoliths in the Staroye Pesyanoe aubrite. *LPSC 42nd*, # 1612.
7. Kolesov G. M., Shubina N. A., Lyul A. Yu. (2001) Optimizing instrumental neutron activation analysis extraterrestrial materials: fragments of lunar rocks, meteorites, chondrules, and ultrarefractory inclusions. *I. Anal. Chem.*, V. 56, p. 1022-1028.
8. Kasharov L.L., Ivliev A.I., Kalinina G.V., Lavrentjeva Z. A., Lyul A. Yu., Kuynko N. S. (2003). Pre-accretion and/or regolith history of the Pesyanoe obrite matter. *LPSC 34nd*, # 1025
9. Morgan J. W., Jansens M. J., Hertogen J., Gros J., Takanashi H. (1979). Ries impact crater, Sout hern Germany: search for meteoritic material. *Geochim. Cosmochim. Acta*, v. 43, p. 803 – 815.
10. Wolf R., Woodrow A., Anders E. (1979). Lunar basalts and pristine highland rocks: comparison of siderophile and volatile elements, *Proc.10 th Lunar. Planet. Sci. Conf.*, p. 2107-2130.
11. Wolf R., Anders E. (1980). Moon and Earth: compositional differences inferred from siderophiles, volatiles, and alkalis in basalts. *Geochim. Cosmochim. Acta*, v. 44, p. 2111-2124.
12. Wheelock M.M., Heavilon C.F., Keil K. (1990). An ion microprobe study of REE distributions in sulfide silicate minerals in the Norton Couty aubrite. *Lunar Planet. Sci. Conf. XXI*, p. 1327-1328.
13. Floss Ch., Strait M. M., Crozaz G. (1990). Rare earth elements and the petrogenesis of aubrites. *Geochim. Cosmochim. Acta*, v. 54, p. 3553-3558.
14. Floss Ch., Crozaz G. (1993). Heterogeneous REE patterns in oldhamite from aubrites: their nature and origin. *Geochim. Cosmochim. Acta*, v. 57, p. 4039-4057.

15. Graham A. L., Henderson P. (1985). Rare earth element abundances in separated phases of Mayo Belwa an enstatite achondrite. *Meteoritics*, v. 20, p. 141-149.

Ustinova G. K. Isotopic relations in reservoirs of condensation of the primordial matter

V. I. Vernadsky Institute of Geochemistry and Analytical Chemistry RAS, Moscow

Abstract. Probable zones of condensation of the primordial matter in the early Solar system, e. g. in various regions of protosolar nebula or in supernova remnants could be different by their radiation conditions, in which spallation reactions work. Isotopic relations of the spallation reaction products highly depend on radiation conditions, and, therefore, may be used as isotopic indicators of the regions of their production and subsequent condensation of the most refractory mineral grains bearing them. Search and analysis of the isotopic relations in the early condensates of meteorites of different chemical groups provide us to identify the ranges of formation of their parent bodies.

Key words: early Solar system, spallation reactions, isotopic anomalies, early condensates, meteorites, parent bodies.

Citation: Ustinova, G. K. (2014). Isotopic relations in reservoirs of condensation of the primordial matter. *Experimental geochemistry*. V. 2. No.

Introduction: The isotopic anomalies of some extinct radionuclides testify to the outburst of a nearby supernova just before the collapse of the protosolar nebula. Therefore, there were, at least, two reservoirs of condensation of the primordial matter: expanding shell of the supernova and main volume of the protosolar nebula. They are different in two aspects.

1. Composition. The protosolar nebula consisted of the matter of a giant gas–dust cloud, the ultrasonic turbulence of which homogeneously mixed the matter with the nucleosynthesis products of approximately ten supernovae during the nebula lifetime until its collapse into the protosun [Lada, Shu,1990]. The matter of expanding shell of the last supernova, before the complete mixing with that of the protosolar cloud, was enriched with products of nucleosynthesis, which depend on the type of supernova. If it was a core-collapse Sn II, its shell would be enriched, in particular, with the products of *r*-process. In the case of carbon-detonation Sn Ia, at the explosive burning of carbon and oxygen only elements of intermediate atomic weights (up to iron peak) were synthesized, e.g. from 0.6 to 0.8 M_{\odot} of the iron group elements, and ~ 0.3 M_{\odot} of Si and other elements, including Mg, P, S, and Ca. [Gameso et al. 2005] The expanding zone of the complete destruction of Sn Ia is depleted by the burnt out C and O; besides, the products of *r*-process are absent. In the well-mixed matter of the protosolar nebula the isotopic anomalies of extinct radionuclides typically show, on logarithmic scale, a linear dependence on the squared half-life of all the radionuclides $(T_{1/2})^2$ [Cameron, Lodders, 2004]. However, in minerals of CAIs with a formation interval of ≤ 1 m.y., a large excess of short-lived radionuclides only, the mass of which is less than the mass of iron-peak nuclei, is observed in addition to the radionuclides captured from the nebula (and corresponding to $(T_{1/2})^2$) [Lodders, Cameron, 2004]. That might happen only after a SN Ia explosion [Ustinova, 2006].

2. *Radiation conditions.* Other sources of isotopic anomalies were spallation reactions with high-energy particles accelerated in shock waves [Ustinova, 2013a]. The region of a supernova outburst is a zone of strong shock waves, at the front of which the diffusive acceleration of particles with formation of the power-law energy spectrum of high hardness

$$F(>E_0) \sim E^{-\gamma}$$

takes place [Berezko, Krymsky, 1988]. Here the spectral index is $\gamma = (\sigma + 2)/(\sigma - 1)$, where σ is the degree of matter compression at the shock front. Obviously, in strong shock waves (at $\sigma \gg 1$), a very hard spectrum of accelerated particles (with $\gamma \rightarrow 1$) can be formed. As a result, the fluxes of nuclear-active particles above the threshold energies of spallation reactions can increase up to two orders of magnitude in comparison with the average integral fluxes of $\sim 10^{19} \text{ cm}^{-2}$, predicted for the early Solar system [Audouze, 1970]. Besides, since the energy spectrum of nuclear-active particles changes, the weighted spectrum-averaged cross sections

$$\bar{\sigma} = \frac{\int_{E_0}^E \sigma(E)F(E)dE}{\int_{E_0}^E F(E)dE}$$

for the production of many isotopes, the excitation functions of which are sensitive to the shape of the particle spectrum, vary as well. Hence, owing to the diffusive shock wave acceleration of particles, the spallation production rates for all the isotopes must increase, but the rate of the increase is not the same for different isotopes. In other words, in reservoirs reprocessed by shock waves (expanding shells of supernovas) isotopic and elemental ratios being absolutely different from those in the matter not affected by such reprocessing (the main volume of the protosolar nebula) are formed [Ustinova, 2007a; 2013a].

Isotopic Relations: It is important that the quantities of such isotopic anomalies can be exactly calculated. Table1 presents the isotopic relations of $^{26}\text{Al}/^{27}\text{Al}$, $^{41}\text{Ca}/^{40}\text{Ca}$ and $^{53}\text{Mn}/^{55}\text{Mn}$, formed in spallation reactions of high-energy particles of the different energy spectrum hardness (different γ) with some corresponding target nuclei in the early Solar system. The cosmic abundances of the target elements from [Anders, Grevesse, 1989] were used. Experimental and simulated excitation functions of the considered isotopes from their nearby target nuclei were compiled from many papers, the references to which were given in previous works, e.g. [Ustinova, 2007a; 2013a].

Table 1. Dependence of isotopic ratios on the hardness of the energy spectrum (γ) of incident particles

Isot.ratio γ	$^{26}\text{Al}/^{27}\text{Al}$ 10^{-5}	$^{41}\text{Ca}/^{40}\text{Ca}$ 10^{-6}	$^{53}\text{Mn}/^{55}\text{Mn}$ 10^{-4}
1.1	15.76	0.7025	30.39
1.5	6.98	0.3451	14.06
2	0.594	0.1043	3.94
2.5	0.46	0.08073	1.00
3	0.093	0.00852	0.248
3.5	0.023	0.00229	0.0615
4	0.0059	0.000672	0.01702
5	0.00035	0.000043	0.00124
6	0.00002	0.000003	0.00009

The hard energy spectrum of particles is a very important characteristic of radiation from the star formation regions reproduced by the strong shock waves: the index of the integral spectrum may decrease down to $\gamma \sim 1$ as compared with $\gamma \sim 2.5$ in galactic cosmic rays and $\gamma \sim 3-6$ in solar cosmic rays. Measuring the isotopic ratios in a refractory meteoritic mineral one may estimate the radiation conditions in its condensation reservoir, i.e. identify the latter. It is clear that such a quantitative approach provide us with subtle tool for studying peculiarities of formation of the primordial matter and the bodies in the early Solar system.

Discussion: It is clear that, due to the supersonic turbulent mixing, the high anomaly isotopic ratios, as well as unusual composition of the expanding supernova shells, will be diluted and lost among the tremendous quantity of the common isotopic ratios in the main volume of the protosolar nebula. However, during expansion, the newly synthesized matter of supernova was cooled at the periphery of its shell, so that the early high-temperature condensates might capture the isotopes with their

anomalous relations, formed in this region, and might conserve them further in the primordial matter. It is worth noting here that D. D. Clayton [Clayton, 1978] was, apparently, the first to indicate that the time between the generation of isotopes and their fixation in solid phases is the most cryptic and least studied period in cosmochemistry. The nature and the amount of each specific isotope anomaly in a certain mineral phase were determined by the ability of isotopes to survive and by the ability of the given mineral to retain these isotopes under the extreme *PT*-conditions (pressure and temperature conditions) of the early Solar System. Indeed, just in high-temperature phases of some refractory minerals of CAI in the carbonaceous chondrites the anomalous isotopic relations, formed in hard radiation conditions ($\gamma < 2$), are observed [Wasserburg, 1985; Lewis et al., 1990; Srinivasan et al., 1996; etc.]. This allows us to suppose that just the peripheric layers of the supernova expanding shell were zones of condensation of those refractory minerals and formation of CAI of carbonaceous chondrites [Ustinova, 2007b; 2013a].

The most interesting is the situation in differentiated meteorites [Ustinova, 2013b]. The latter bear minerals that were probably condensed under quite different radiation conditions (see Fig.1).

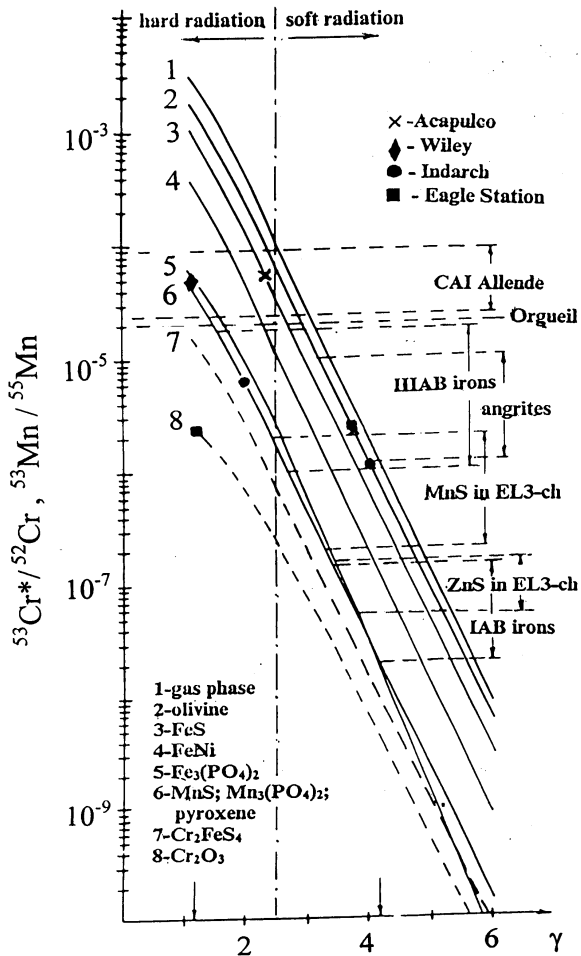


Fig. 1. Formation of $^{53}\text{Mn}/^{55}\text{Mn}$ (solid curves) and $^{53}\text{Cr}^*/^{52}\text{Cr}$ (dashed curves) ratios in the protosolar gas–dust cloud at various values of the spectral index γ for accelerated particles. The curves for ^{53}Mn were calculated for the formation in (1) gas phase and minerals: (2) olivine, (3) troilite, (4) nickel–iron, (5) iron orthophosphates, (6) alabandite (similarly in manganese orthophosphates and pyroxene), (7) daubreelite, and (8) chromite. The references on experimental levels in CAI of the Allende carbonaceous chondrite, Orgueil carbonaceous chondrite, graffonite of iron meteorites, olivines of angrites, alabandite and sphalerite of enstatite chondrites, and alabandite of iron meteorites are cited in [Ustinova, 2013a]. The cross, diamond, circle, and square are the data for the Acapulco, Wiley, Indarch, and Eagle Station meteorites, respectively. The cosmic abundances are taken from [Anders, Grevesse, 1989]. The arrows on the absciss show the observed range of $\gamma \sim 1.2\text{--}4.2$.

The very close ratios $^{53}\text{Mn}/^{55}\text{Mn} \sim (1\text{--}2) \cdot 10^{-6}$ (corresponding to spectral index $\gamma \sim 4$, see Table 1) are observed in the olivines of meteorites with various thermal history (in pallasite, achondrite, enstatite chondrite, and angrite). However, in sulfides and phosphates of the same meteorites, as well as in the Wiley iron meteorite, these ratios are much higher and they correspond to $\gamma \sim 1.2\text{--}2.5$. The striking coexistence of materials from reservoirs with different radiation conditions in the same meteorites

allows us to conclude that the parent bodies of differentiated meteorites probably were formed in the zones of the most efficient mixing of the matter of a dust-rich (including ^{26}Al) supernova envelope and of the major reservoir of the protosolar nebula strongly enriched with dust too. Just the decay of simultaneously trapped ^{26}Al promotes heating of the matter and further magmatic processes in differentiated meteorites.

A question arises why just sulfides and phosphates turned out to be condensates of the supernova reservoirs. In the case of SnII explosion, all the shells above the neutronized core were thrown away with the nearest one enriched by the products of oxygen burning, namely, Si, P and S [Barnes, 1982]. Just that shell underwent the highest compression and the hardest irradiation with the shock wave accelerated particles. The chemical form of the matter in that shell are just sulfides and phosphates [Clayton, 1981]. In the case of Sn Ia complete destruction, induced by the explosive C and O burning, the matter was condensed under gradual cooling at very reducing medium, strongly depleted in O. Therefore, sulfides and phosphides were the most favored condensates. Phosphates are, apparently, the results of subsequent oxidation. It is important that the P-bearing Fe–Ni sulfides are found in CM chondrites, and their paragenesis points out to their extrasolar origin [Nazarov et al., 2009].

This work is supported in part by Program 22 of Fundamentals Research of RAS.

References

1. Anders E., Grevesse N. (1989). Abundances of the elements: Meteoritic and solar. *Geochim. Cosmochim. Acta.* v. 53. p. 197-214.
2. Audouze J. (1970). Some nucleosynthetic effects of energetic proton fluxes on stellar surfaces and on the solar system. *Astron. Astrophys.*, v. 8, p. 436-457.
3. Barnes C. A. (1982). Nuclear reactions in highly evolved stars. *Essays in Nuclear Astrophysics* (Cambridge: CUP) p. 193-232.
4. Berezhko E. G., Krymsky G. F. (1988) Acceleration of cosmic rays by shock waves. *Soviet Phys. Uspekhi*, v. 31, p. 27-51.
5. Cameron A. G. W., Lodders K. (2004) Interpretation of the meteoritic extinct radioactivity – mean life relation. *Lunar Planet. Sci. 35th.* (Houston: LPI) Abstract # 1181.
6. Clayton D. D. (1978) Precondensed matter: key to the early solar system. *Moon and Planets*, v.19, p. 109-137.
7. Clayton D. D. (1981) Some key issues in isotopic anomalies: Astrophysical history and aggregation. *Proc. Lunar Planet. Sci.12B* (Houston: LPI), p. 1781-1802.
8. Gamezo V. N., Khokhlov A. M., Oran E. S. (2005). Three-dimensional delayed-detonation model of type Ia supernovae. *Astrophys. J.*, v. 623, p. 337-346.
9. Lada C. J., Shu F. Y. (1990) The formation of sunlike stars. *Science*, v. 248, p. 564-572.
10. Lewis R.S., Amari S., Anders E. (1990). Meteoritic silicon carbide: Pristine material from carbon stars. *Nature*, v. 348, p. 293-298.

11. Lodders K., Cameron A. G. W. (2004) The mean life squared relationship for abundances of extinct radioactivities. *Lunar Planet. Sci.* 35th (Houston: LPI), Abstract #1186.
12. Nazarov M. A., Kurat G., Brandstaetter F., Ntaflou T., Chaussidon M., Hoppe P. (2009). Phosphorus-Bearing Sulfides and Their Associations in CM Chondrites. *Petrology*, v. 17, p. 101-123
13. Srinivasan G., Sahupal S., Ulyanov A.A., Goswami J.N. (1996). Ion microprobe studies of Efremovka CAIs: II. Potassium isotope composition and ⁴¹Ca in the early solar system. *Geochim. Cosmochim. Acta*, v. 60, p. 1823-1835.
14. Ustinova G. K. (2006). The type Ia supernova and origin of the Solar System. *Met. Planet. Sci.*, 41 (Suppl), p. A177, Abstract #5045.
15. Ustinova G. K. (2013a). Spallation reactions in shock waves at supernova explosions and related problems. *Phys. Atom. Nucl.*, v. 76, p. 616-655.
16. Ustinova G. K. (2007a) On the problem of Solar System origin: The regularities of noble gas fractionation in shock waves. *Solar Syst. Res.*, v. 41, p. 231-255.
17. Ustinova G. K. (2007b) A radiation criterion of CAI condensation reservoir and origin of the carbonaceous chondrites. *Lunar Planet. Sci.* 38th (Houston: LPI), Abstract #1159.
18. Ustinova G. K. (2013b) Isotopic indicators for zones of condensation of the primordial matter. *Met. Planet. Sci.*, 41 (Suppl), Abstract #5037.
19. Wasserburg G. J. (1985) Short-lived nuclei in the early solar system. *Protostars and Planets II* (Tucson: UAP), p. 703-737.

Shornikov S. I. High temperature thermodynamic study of Ca–Al–inclusion’s compound volatility

Vernadsky Institute of Geochemistry and Analytical Chemistry of RAS, Moscow

Abstract. The comparison of experimental and calculated data on evaporation of compounds forming Ca–Al–inclusions allowed to determine the comparative volatility groups in the temperature range of 1800–2200 K. The compound’s volatilities were calculated also in the temperature range of 1000–1500 K at the oxygen’s low pressure conditions typical for forming of the Ca–Al–inclusion’s minerals. It showed the identity of the compound’s volatility groups at the different redox conditions.

Key words: thermodynamics of evaporation, the CaO–MgO–Al₂O₃–SiO₂ system, Ca–Al–inclusion.

Citation: Shornikov, S. I. (2014). High temperature thermodynamic study of Ca–Al–inclusion’s compound volatility. *Experimental Geochemistry*. Vol. 2. No.

Grossman [Grossman, 1972] developed the physico-chemical model of the substance’s sequence condensation. This model described the origin of chondrites and the Ca–Al–inclusion’s substance and suffered the considerable modifications now [Grossman et al., 2000; Grossman et al., 2008]. The obtained new information on the inclusions in chondrites structure lead to the conceptions that the high temperature evaporation processes played an appreciable role in their forming.

The aim of the present study was the thermodynamic investigation of volatility of basic compounds forming the Ca–Al–inclusion’s substance composition (dmitryivanovite CaAl₂O₄, grossite CaAl₄O₇, hybonite CaAl₆O₁₉, perovskite CaTiO₃, spinel MgAl₂O₄, diopside CaMgSi₂O₆, anorthite CaAl₂Si₂O₈, gehlenite Ca₂Al₂SiO₇ и grossular Ca₃Al₂Si₃O₁₂) at high temperatures – 1800–2200 K. On the base of the thermodynamic study’s results [Shornikov, 2010], it was interesting to apply the observed rules for calculations of these compound’s volatility at conditions typical for the Ca–Al–inclusion’s minerals forming.

The initial data for determination of comparative volatility of listed compounds were the temperature dependences of total vapor pressures over compounds (*p_{tot}*) presented in the fig. 1a. Their values were find as a sum of vapor species partial pressures (*p_i*) of gas phase over these compounds determined experimentally by mass spectrometric Knudsen effusion method [Shornikov, 2010] described in detail earlier [Shornikov et al., 2000]. It is necessary to point that the whole of experiments were carried out at the identical redox conditions (at the compound’s evaporation from molybdenum effusion cells). It allowed to considerate the comparative volatility of compounds correctly [Shornikov, 2008].

By convention we may choose three general groups of compounds on the comparative volatility at the redox conditions presented in the fig. 1a: 1) hard volatile – CaAl₆O₁₉, CaAl₄O₇, CaAl₂O₄, CaTiO₃; 2) middle volatile – Ca₂Al₂SiO₇, MgAl₂O₄; and 3) volatile – CaMgSi₂O₆, Ca₃Al₂Si₃O₁₂, CaAl₂Si₂O₈. This sequence corresponded to the compound’s volatility calculated on thermochemical data [Shornikov, 2004; Shornikov, 2010] for the case of neutral conditions (at the absence of external chemical influence on evaporation) presented on fig. 1b.

We can see in the fig. 1 the differences in the absolute values of total vapor pressure over the compounds obtained at the different redox conditions. It was caused by the heterogeneous reaction



which reduce the oxygen’s partial pressure in the gas phase over the compounds, and correspondingly increase the partial pressures of the oxygen-deficient vapor species and the total vapor pressure finally.

The consideration of experimental temperature dependences of *p_O* over the studied compounds (fig. 2a) showed their coincidence excepting the same for the case of MgAl₂O₄. It is possible, that it caused the high comparative volatility of atomic magnesium containing in the gas phase over spinel. The absence of passing of reaction (1) caused the difference of similar temperature dependences calculated for the case of the absence of external chemical influence (fig. 2b).

The supervision made above about identity of the oxygen’s partial pressure temperature dependences (fig. 2a) allowed to calculate the total vapor pressure values over considered compounds at temperatures of 1000–1500 K at the oxygen’s low pressure conditions (*p_O* = 10⁻¹⁸ atm at 1503 K), that it is typical for the Ca–Al–inclusion’s mineral forming [Grossman et al., 2000; Grossman et al., 2008].

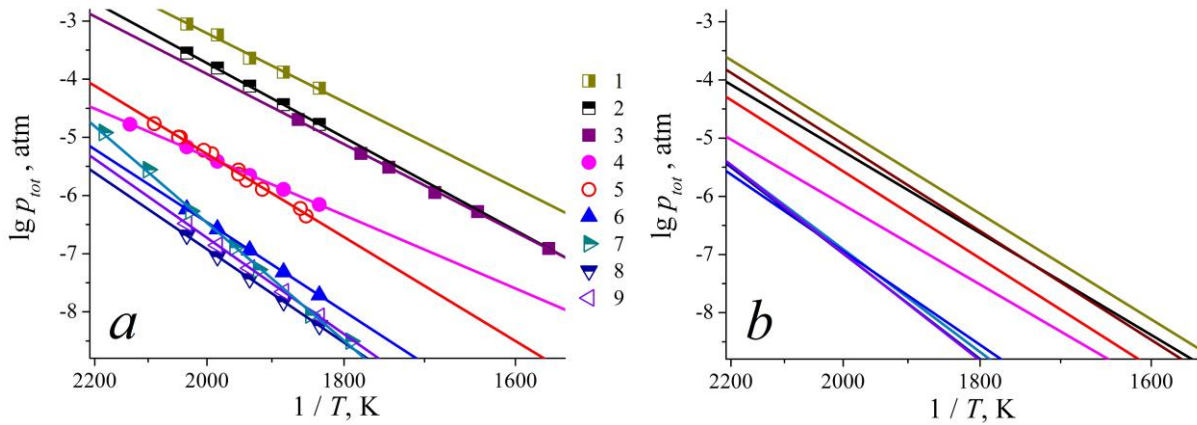


Fig. 1. The total vapor pressure over compounds: (a) determined by mass spectrometric Knudsen effusion method [Shornikov, 2010] at the compound's evaporation from molybdenum cell (1 – $\text{CaAl}_2\text{Si}_2\text{O}_8$, 2 – $\text{Ca}_3\text{Al}_2\text{Si}_3\text{O}_{12}$, 3 – $\text{CaMgSi}_2\text{O}_6$, 4 – $\text{Ca}_2\text{Al}_2\text{SiO}_7$, 5 – MgAl_2O_4 , 6 – CaAl_4O_7 , 7 – CaTiO_3 , 8 – CaAl_4O_7 , 9 – $\text{CaAl}_6\text{O}_{19}$); (b) calculated in the present study using thermochemical data [Shornikov, 2010] at the absence external chemical influence, presented the lines of the same color.

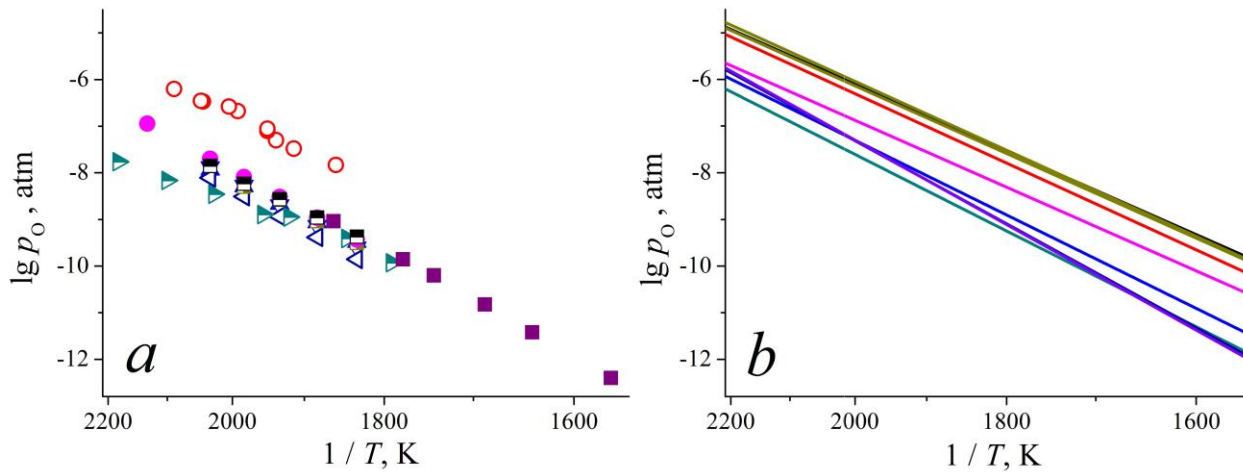


Fig. 2. The partial pressure of atomic oxygen over the compounds: (a) determined by mass spectrometric Knudsen effusion method [Shornikov, 2010] at the compound's evaporation from molybdenum cell (1 – $\text{CaAl}_2\text{Si}_2\text{O}_8$, 2 – $\text{Ca}_3\text{Al}_2\text{Si}_3\text{O}_{12}$, 3 – $\text{CaMgSi}_2\text{O}_6$, 4 – $\text{Ca}_2\text{Al}_2\text{SiO}_7$, 5 – MgAl_2O_4 , 6 – CaAl_4O_7 , 7 – CaTiO_3 , 8 – CaAl_4O_7 , 9 – $\text{CaAl}_6\text{O}_{19}$); (b) calculated in the present study using thermochemical data [Shornikov, 2010] at the absence external chemical influence, presented the lines of the same color.

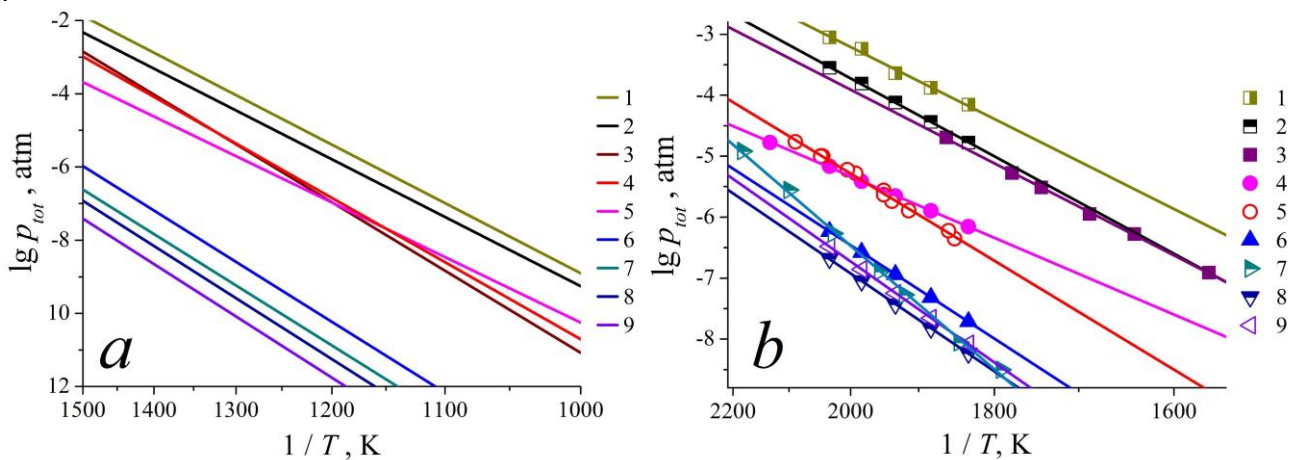


Fig. 3. The total vapor pressure over compounds: (a) calculated at the oxygen's low pressure conditions typical for forming of the Ca–Al–incusion's minerals [Grossman et al., 2000; Grossman et al., 2008] and (b) determined experimental by mass spectrometric Knudsen effusion method [Shornikov, 2010] at the compound's evaporation from molybdenum cell. Table of symbols: 1 – $\text{CaAl}_2\text{Si}_2\text{O}_8$, 2 – $\text{Ca}_3\text{Al}_2\text{Si}_3\text{O}_{12}$, 3 – $\text{CaMgSi}_2\text{O}_6$, 4 – $\text{Ca}_2\text{Al}_2\text{SiO}_7$, 5 – MgAl_2O_4 , 6 – CaAl_4O_7 , 7 – CaTiO_3 , 8 – CaAl_4O_7 , 9 – $\text{CaAl}_6\text{O}_{19}$.

The calculation showed (fig. 3a) the saving of the studied compound's volatility sequence as in the case of high temperature – 1800–2200 K (fig. 3b) at the saving of the relation of absolute values of the total vapor pressures over compounds.

Thus, the comparison of experimental and calculated data on evaporation of compounds forming Ca–Al–inclusions allowed to set the comparative volatility groups in the temperature range of 1800–2200 K: 1) CaAl₆O₁₉, CaAl₄O₇, CaAl₂O₄, CaTiO₃; 2) Ca₂Al₂SiO₇, MgAl₂O₄; 3) CaMgSi₂O₆, Ca₃Al₂Si₃O₁₂, CaAl₂Si₂O₈.

The compound's volatilities were calculated also in the temperature range of 1000–1500 K at the oxygen's low pressure conditions typical for forming of the Ca–Al–inclusion's minerals. It showed the identity of the compound's volatility groups at the different redox conditions.

References

- Grossman, L. (1972). Condensation in the primitive solar nebula. *Geochim. Cosmochim. Acta*, vol. 36, no. 5, pp. 597–619.
- Grossman, L., D. S. Ebel, S. B. Simon, A. M. Davis, F. M. Richter, N. M. Parsad (2000). Major element chemical and isotopic compositions of refractory inclusions in C3 chondrites: the separate roles of condensation and evaporation. *Geochim. Cosmochim. Acta*, vol. 64, no. 16, pp. 2879–2894.
- Grossman, L., S. B. Simon, V. K. Rai, M. H. Thiemens, I. D. Hutcheon, R. W. Williams, A. Galy, T. Ding, A. V. Fedkin, R. N. Clayton, T. K. Mayeda (2008). Primordial compositions of refractory inclusions. *Geochim. Cosmochim. Acta*, vol. 72, no. 12, pp. 3001–3021.
- Shornikov, S. I., I. Yu. Archakov, T. Yu. Chemekova (2000). Mass spectrometric study of evaporation processes and phase relation in the Al₂O₃–SiO₂ system. *Russ. J. Phys. Chem.*, vol. 74, no. 5, pp. 775–782.
- Shornikov, S. I. (2004). A thermodynamic regularities of evaporation processes of CMAS compounds. *Lunar Planet. Sci.*, vol. 35, abstract no. 1058.
- Shornikov, S. I. (2008). The influence of redox conditions on the evaporation of oxide melts of the CaO–MgO–FeO–Al₂O₃–SiO₂ system. *Geochim. Int.*, vol. 46, no. 7, pp. 780–786.
- Shornikov, S. I. (2010). Mass spectrometric Knudsen effusion method: a study of the CaO–MgO–Al₂O₃–SiO₂ system at high temperatures. *XVI Russian conference on experimental mineralogy*, pp. 287–289 [in Russian].

Yurkovets V.P. Shock microstructures in the rocks of Ladoga IVS

The Academy of DNA Genealogy, Boston, USA

Abstract. Along with the "classic" shock-metamorphic features a microscopic shock structures are detected in the rocks of the Ladoga impact-volcanic structure (IVS). Shock microstructures mostly are concentric crushing and melting zones in the grains of target minerals. Fragments of crushed moissanite in a form of fine fraction (less 0.02 mm), or in the form of bigger (up to 0.16 mm)

roundish isometric grains usually are present in the center of the shock microstructures. In some cases, opaque magnetic microspheres are found in centers of the shock microstructures. Their material composition needs a special study.

Key words: Ladoga impact-volcanic structure, shock microstructures, moissanite, magnetic microspheres, impact melt rock, allogenic breccia, impact metamorphism.

Citation: Yurkovets, V.P. (2014). Shock microstructures in the rocks of Ladoga IVS. *Experimental geochemistry*. V. 2. №

The paper presents some evidence of impact origin of the deep part of Lake Ladoga in the framework of impact-volcanic model [Yurkovets, 2014].

The petrographic material that points to impact origin of the deep part of Lake Ladoga, was found on its west coast (Fig. 1, a-d). Crater rim of the Ladoga Impact Volcanic Structure was mapped onshore here. Specimens with evidence of impact metamorphism were also found in southern Ladoga in the material that was transported by glacial and was accumulated in Kirsino's and Shapki's kams (Fig. 1, e,f).

Some examples of "classic" features of impact metamorphism, discovered in rocks of the Ladoga IVS, are shown in Fig. 2.

This are planar deformation features in relict quartz grains of inclusions in impact melt rock (Fig. 2a), planar deformation features in the quartz of shale (Fig. 2b), planar deformation features in the quartz sandstone of allogenic breccia (Fig. 2, bottom series, right), the isotropization - mosaic extinction and kink bands in quartz (Fig. 2, bottom series). The quartz grains with impact spallation [Ernstson, Claudin, 2014] are presented in Fig. 2c and Fig. 2d.

Fig. 3 shows the morphology of the shock microstructures(ShM). Their origin are accompanied by the formation of concentric (all photos in Fig. 3), sometimes planar (photo «b» in Fig. 3) fractures, shock melting (bottom series in Fig. 3) in the mineral grains of the target.

Sometimes opaque magnetic microspheres (photo «b», «a» in the top series of Fig. 3, the left pair in the bottom series of Fig. 3) are at the center of the ShM. In this case, only impact melting of a target grains are observed inside of ShM. Either there are zones of crushing surrounded by shock melting zones of the target mineral (right pair on the bottom series of Fig. 3). In this case, usually moissanite having a high relief, sharp shagreen surface and pearl interference colors is detected in the center of such microstructures (Fig. 4).

Moissanite is usually fractured too. Sometimes moissanite is a whole rounded grains (Fig. 4, middle pair), which are surrounded by relatively weakly disrupted mineral grains of target.

Material composition of opaque magnetic microspheres needs special study.

Sometimes, most often in ferrian inclusions, but not only, ShM overlap. In Fig. 3c we can see two or three ShM overlapping. In Fig. 3d it can be seen overlapping shock microstructures formed by opaque magnetic microspheres.

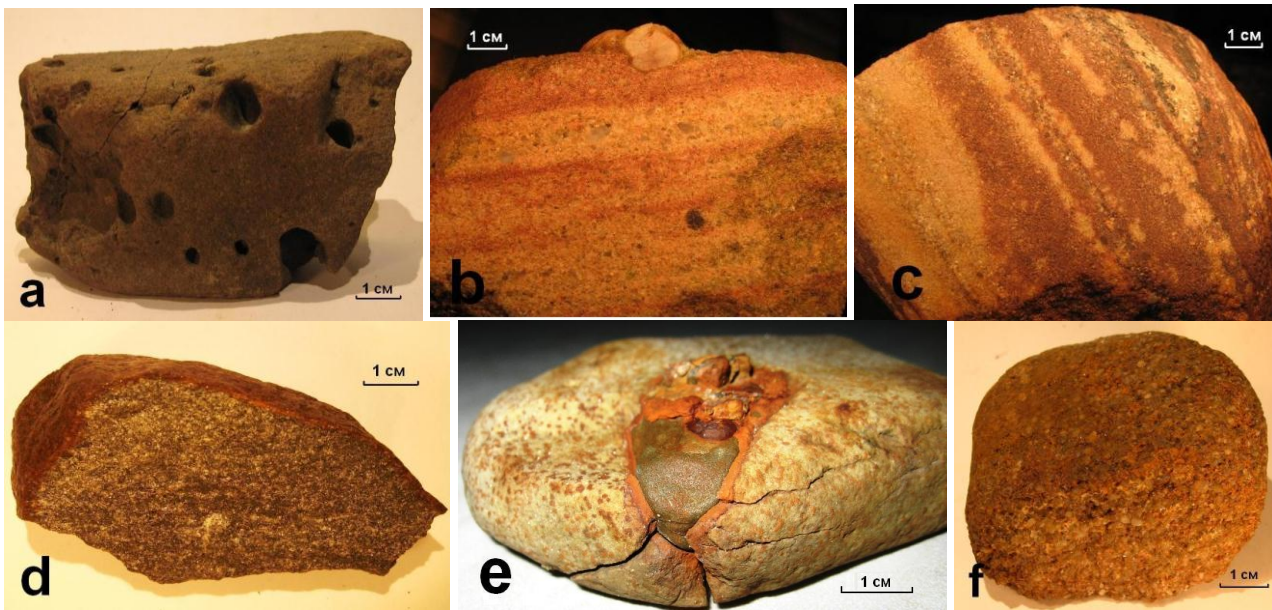


Fig. 1. Specimens having shock-metamorphic features

a – impact melt rock, cape Vladimirovakiy; b – fragment of allogenic breccia, cape Vladimirovakiy; c – fragment of allogenic breccia, mouth of the river Vuoksa, Priozersk; d - sample of shale melted off, village Beregovoe; e – Cambrian sandstone with ferrian inclusion, village Kirsino; f – ferrian inclusion in Vendian sandstone, village Kirsino.

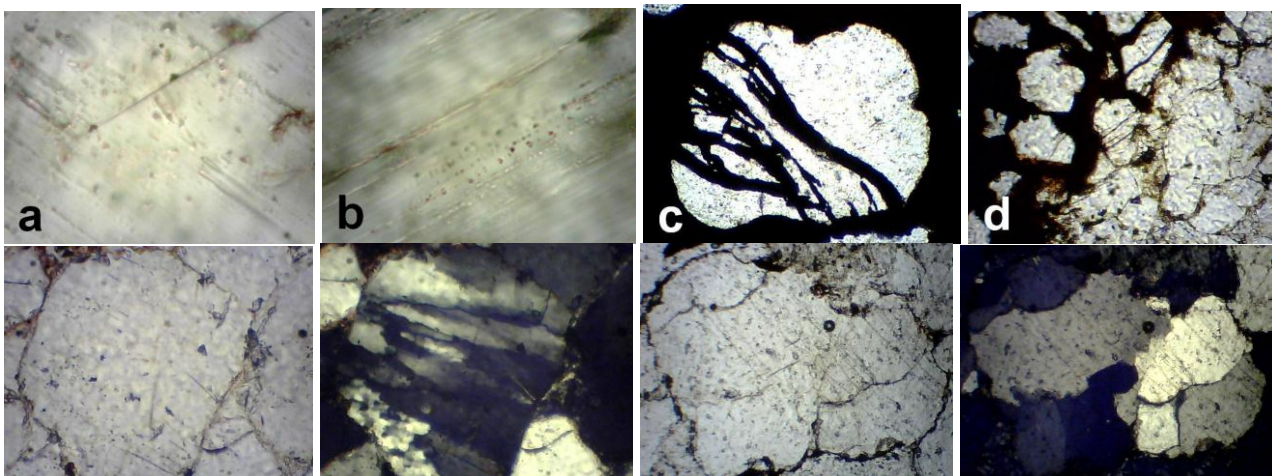


Fig. 2. Impact metamorphic features in the rocks of the Ladoga IVS

Top series: a - thin section № 3, planar deformation features in quartz inclusions within inclusions in impact melt rock, cape Vladimirovskiy; b - thin section № 1a, planar deformation features in quartz of shale from ejecta layer, village Beregovoe; c - thin section № 4, impact spallation in quartz of ferrian inclusion in Vendian sandstone, village Kirsino; d - thin section № 259, impact spallatoin in quartz of ferrian inclusions in Cambrian sandstone, village Kirsino. Plane polarized light.

Bottom series: left pair - thin section № 1; isotropization: strongly mottled extinction pattern (mosaicism) and kink bands in a quartz of Vendian sandstone from allogenic impact breccias, cape Vladimirovskiy. Plane polarized light (left) and xx nicols.

Bottom series: right pair – thin section № 2; planar deformation features in a quartz of Vendian sandstone from allogenic impact breccias, mouth of the river Vuoksa, Priozersk. Plane polarized light (left) and xx nicols.

Field width 0.07 mm (a, b); 0.28 mm (the rest).

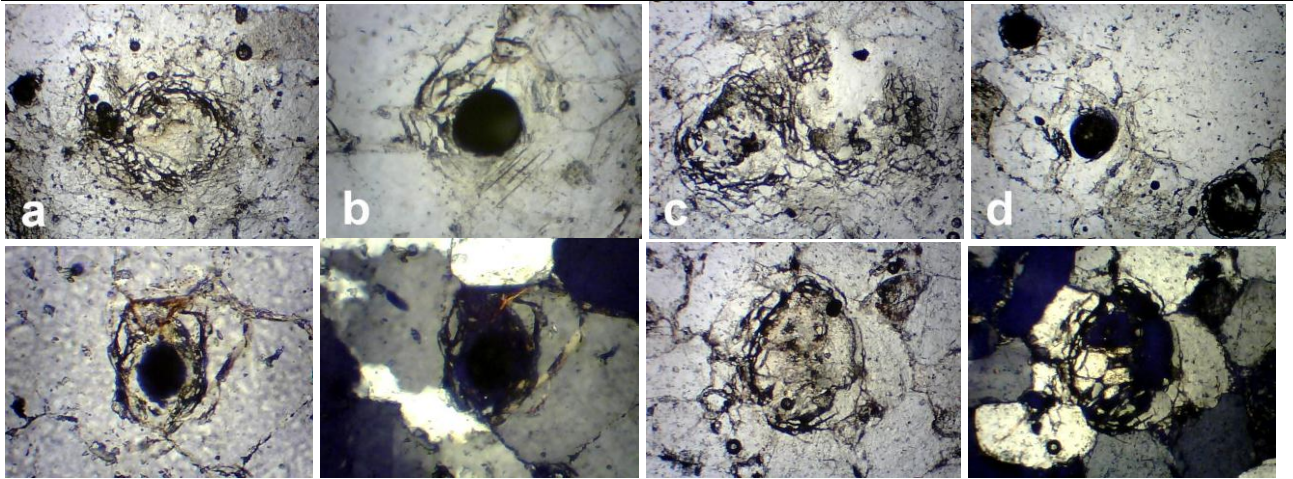
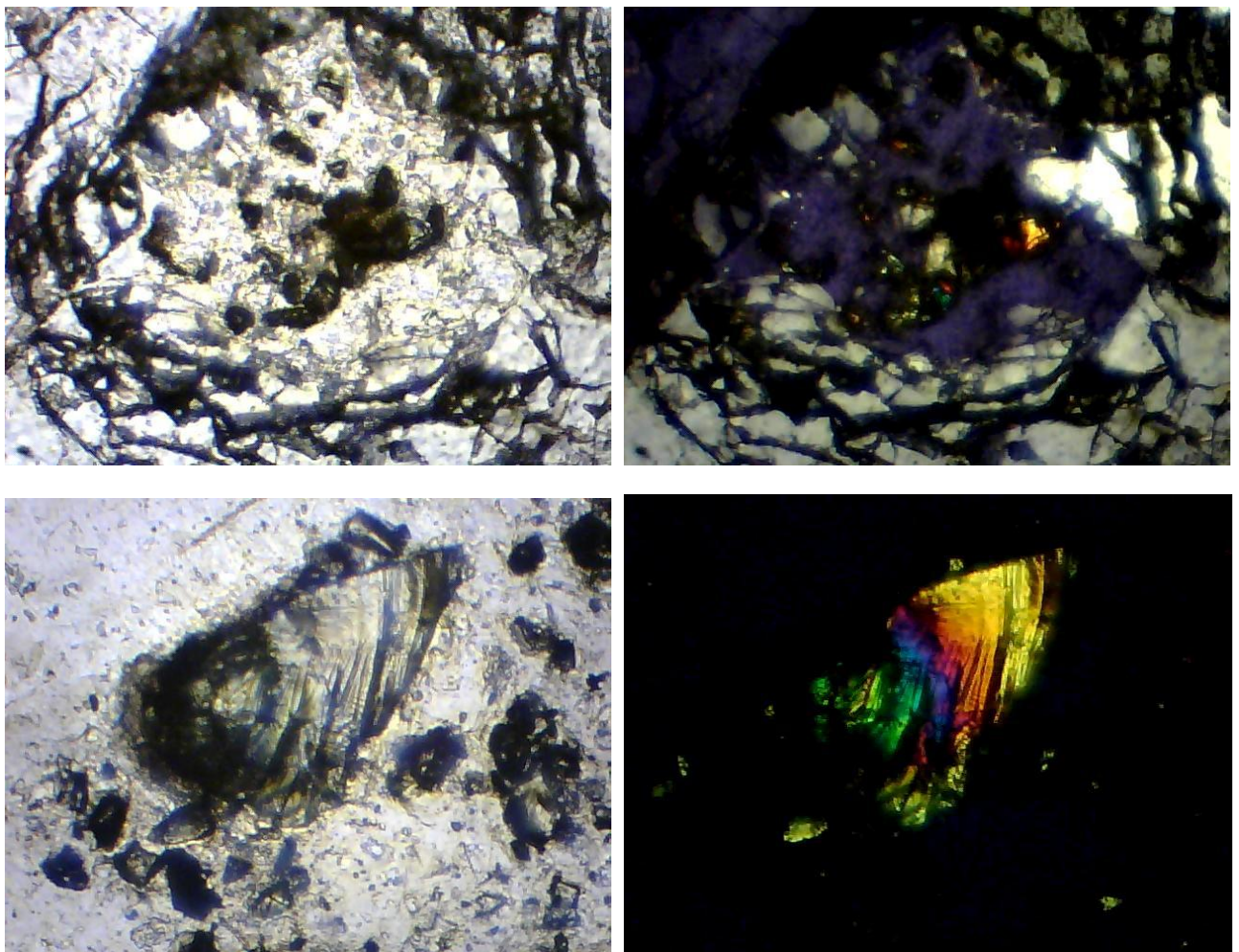


Fig. 3. Morphology of shock microstructures

Upper series: a-d – thin section № 1, shock microstructures, cape Vladimirovskiy. Plane polarized light. Field width 0.9 mm (a,c,d), 0.28 mm (b). Bottom series: left pair – thin section № 1, shock melting in the quartz grain, cape Vladimirovskiy. Plane polarized light (left) and xx nicols. Field width 0.28 mm. Bottom series: right pair – thin section № 2, Splitting and impact melting in the quartz grain, mouth of the river Vuoksa, Priozersk. Plane polarized light (left) and xx nicols. Field width 0.28 mm.



Abstracts

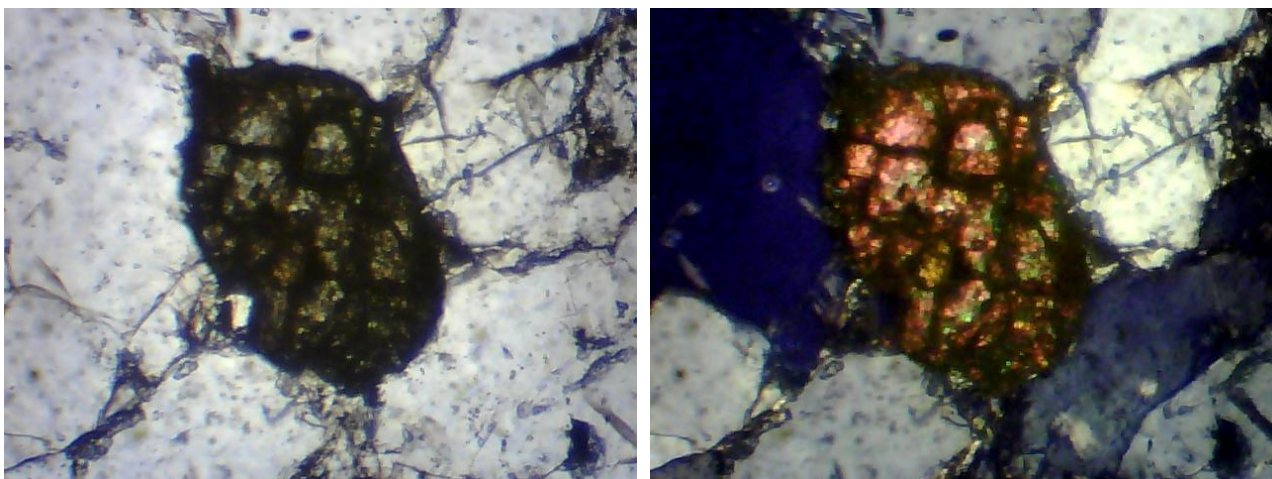
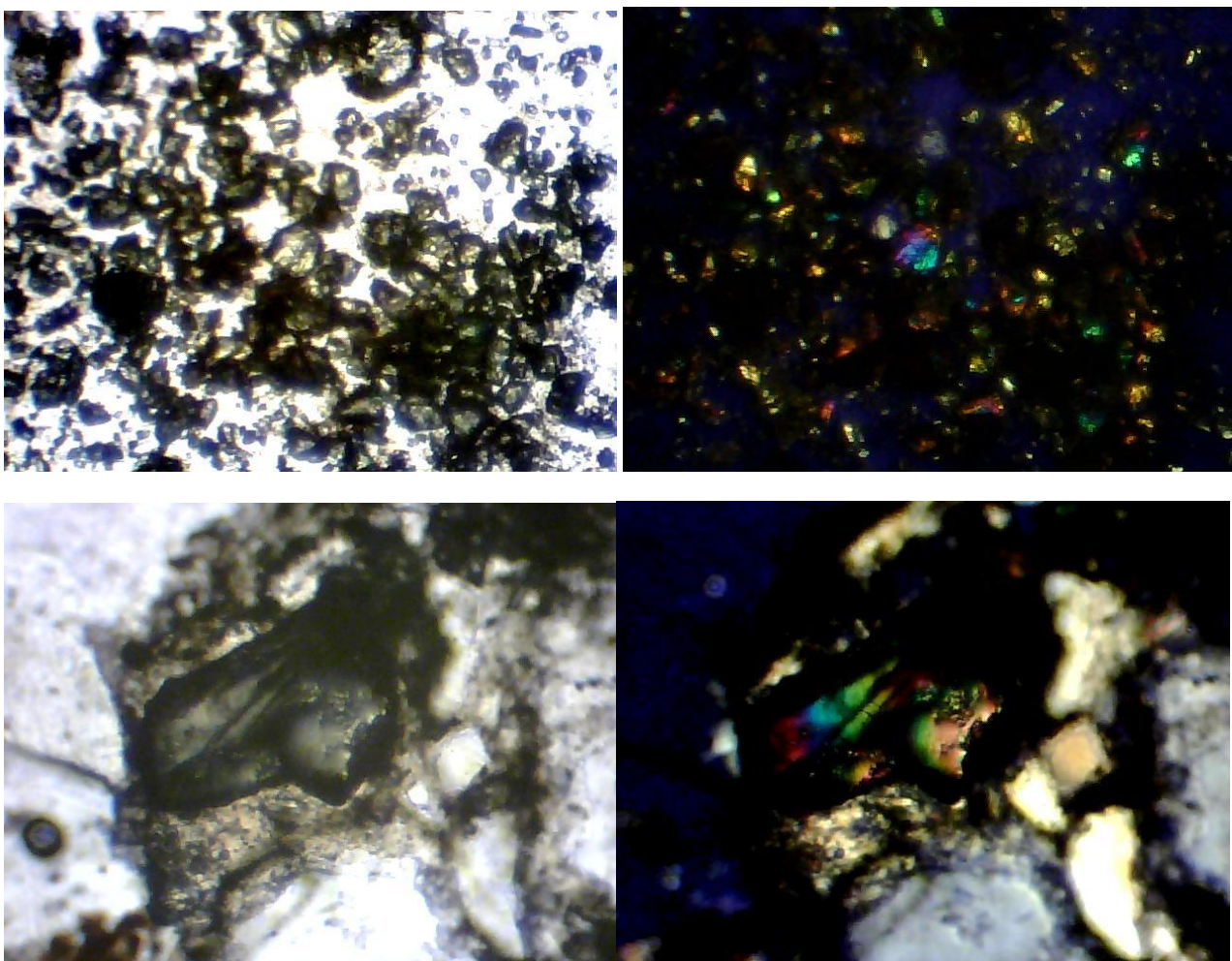


Fig. 4. Moissanite in the center of shock microstructures

Upper pair – thin section № 1, shock microstructure from Fig. 3c (left) in higher magnification, there are moissanite grain in the center, cape Vladimirovskiy. Plane polarized light (left) and xx nicols. Field width 0.28 mm.

Middle pair – thin section № 13, splitting site with a large (about 0.16 mm) moissanite fragment, village Kirsino. Plane polarized light (left) and xx nicols. Field width 0.28 mm.

Bottom pair – thin section № 2, big (about 0.15 mm) roundish moissanite grain, mouth of the river Vuoksa, Priozersk. Plane polarized light (left) and xx nicols. Field width 0.28 mm.



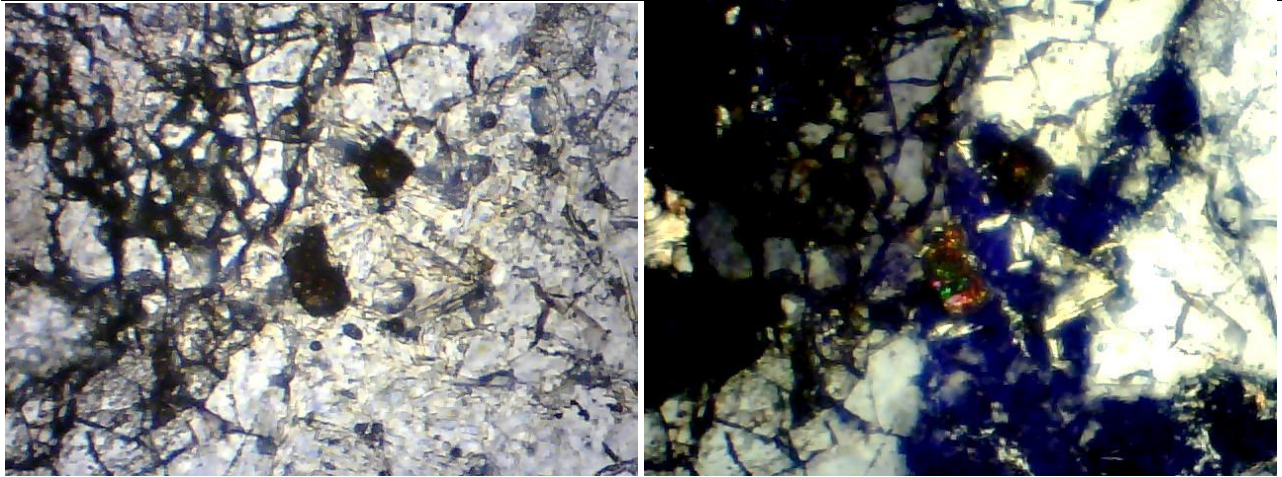


Fig. 5. Fields of crushing formed by the shock microstructures

Upper pair. Thin section № 5, field of crushing with moissanite, village Kirsino.

Middle pair. Thin section № 13, big (about 0.12 mm) moissanite grain, village Kirsino.

Bottom pair. Thin section № 2, part of the field of crushing with the roundish (to 0.05 mm) moissanite grains, mouth of the river Vuoksa. Plane polarized light (all left) and xx nicols. Field width 0.28 mm.

In some cases, a few relatively big ShM form the microfields of crushing and melting, that are too large to fit in the camera angle (Fig. 4 and 5).

Figure 5 (top pair), you can see the field of the crushing formed by small (less than 0.02 mm) grains of crushed moissanite. In the bottom pair there are bigger (about 0.05 mm) roundish moissanite grains, surrounded by relatively weakly broken quartz grains. Big (about 0.12 mm) moissanite grain is shown in the middle pair.

In Fig. 4 (middle pair) and Fig. 5 (middle pair) fragments of the crushing microfield with moissanite are shown. This is the most representative ShM. This ShM occupies on thin section a plot of approximately 3,5 x 3, 5 mm. This thin section was analyzed by electron microprobe and X-ray diffraction analysis, which showed the presence in the site only quartz and moissanite.

References

1. Ernstson K., Claudin F. (2011). Impact spallation in nature and experiment. ERNSTSON CLAUDIN IMPACT STRUCTURES – METEORITE CRATERS. <http://www.impact-structures.com/2011/12/impact-spallation-in-nature-and-experiment/>
2. Yurkovets, V.P. (2014). Shock-metamorphic Features in the Ladoga Impact Volcanic Structure. Proceedings of the Academy of DNA Genealogy. (ISSN 1942-7484). Raleigh, N.C., Lulu. T.7 №2. C. 263-302.

Yakovlev O. I., Shornikov S. I. Thermodynamics and origin of complicated oxide molecules in gaseous phase

V. I. Vernadsky Institute of Geochemistry and Analytical Chemistry RAS, Moscow

Abstract. Knudsen cell vaporization method permitted to study molecular oxide forms in the CaO–MgO–Al₂O₃–TiO₂–SiO₂ system. The vaporization of mullite Al₆Si₂O₁₃, spinel MgAl₂O₄, perovskite CaTiO₃ in dependence on temperature showed that the clusters or complicated molecular forms appeared at high

temperature (1900–2000 K) and their contents increased with temperature increasing.

Key words: vaporization, Knudsen cell method, molecular form.

Citation: Yakovlev, O. I., S. I. Shornikov (2014)/ Thermodynamics and origin of complicated oxide molecules in gaseous phase. *Experimental Geochemistry*, V. 2. №

The complicated molecular forms or molecular clusters in gaseous phase are often observed at high temperatures at vaporization process. Often these clusters consist of sharply fugacity different elements and oxides that might lead to joint vaporization of both the fugacity and nonfugacity matters. That is why the cluster vaporization may play important role in the element distribution between gaseous and condense phases at high temperature processes in particular at impact vaporization and the formation of the chondrules and Ca–Al–inclusions in chondrites.

We studied regularities of the cluster origin during high temperature vaporization of the compounds in the CaO–MgO–Al₂O₃–TiO₂–SiO₂ system that are mullite (Al₆Si₂O₁₃), spinel (MgAl₂O₄), and perovskite (CaTiO₃). The data were obtained by Knudsen effusion mass spectrometric method. The particular attention was attracted to study the dependence the cluster partial pressures and contents on the temperatures. These dependences are shown in fig. 1 [Shornikov et al., 1994; Shornikov, 2001; Shornikov, 2013]. It is interesting to note that the points of melt temperatures of the minerals (mullite – 2180±10 K, spinel – 2388±15 K, perovskite – 2243±5 K [Chase, 1998]) were higher than experimental temperatures that means the vaporization occurred from the crystal state.

The study of the vapor components showed general regularity that the complicated molecular forms appeared in gaseous phase exceptionally at very high vaporization temperatures ($T > 1900\text{--}2000\text{ K}$). Besides the experimental data have unambiguously shown that the contents of the complicated molecular forms – AlSiO (fig. 1 a, d; line 4), MgAlO (fig. 1 b, e; line 4) and CaTiO₃ (fig. 1 c, f; line 6) increased with increasing temperature.

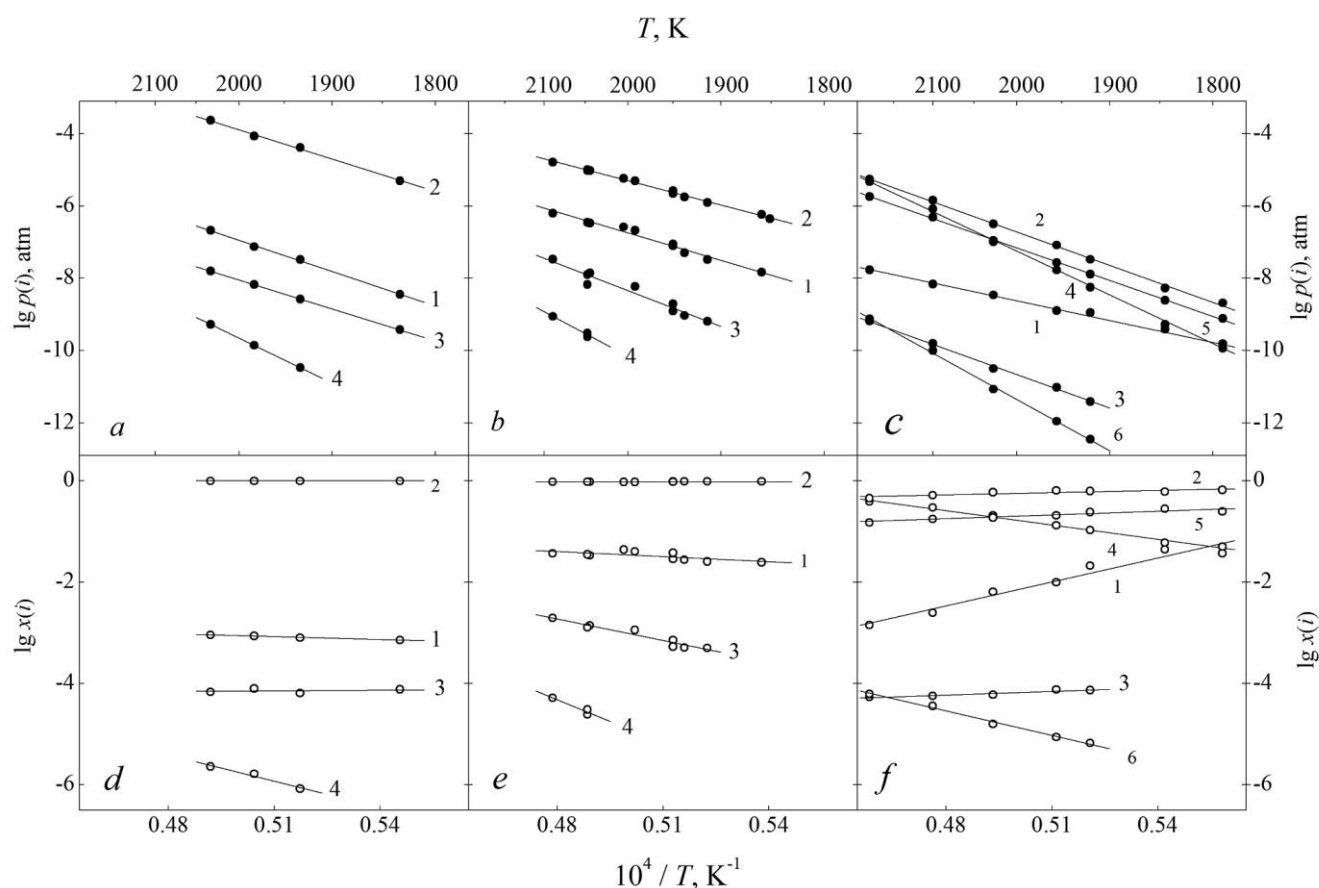


Fig. 1. Partial pressure (a, b, c) and contents (d, e, f) of vapor components above minerals oxides: mullite (a, d: 1 – O, 2 – SiO, 3 – Al, 4 – AlSiO; spinel (b, e): 1 – O, 2 – Mg, 3 – AlO, 4 – MgAlO; perovskite (c, f): 1 – O, 2 – Ca, 3 – CaO, 4 – TiO, 5 – TiO₂, 6 – CaTiO₃).

Table 1. Evaporation reactions and their enthalpy values at 2000 K.

Mullite Al ₆ Si ₂ O ₁₃	$\Delta H_r(T)$, kJ/mole
$1/2[Al_2O_3] = (Al) + 3/2(O)$	1528±1
$[SiO_2] = (SiO) + (O)$	1043±1
$1/2[Al_6Si_2O_{13}] = (AlSiO) + 2(Al) + 5.5(O)$	5332±26
$(Al) + (SiO) = (AlSiO)$	-314±26
$(AlO) + (Si) = (AlSiO)$	-582±20
Spinel MgAl ₂ O ₄	$\Delta H_r(T)$, kJ/mole
$[MgO] = (Mg) + (O)$	986±1
$1/2[Al_2O_3] = (Al) + 3/2(O)$	1528±1
$[MgAl_2O_4] = (MgAlO) + (Al) + 3(O)$	3291±32
$(Mg) + (AlO) = (MgAlO)$	-213±35
$(MgO) + (Al) = (MgAlO)$	-387±34
Perovskite CaTiO ₃	$\Delta H_r(T)$, kJ/mole
$[CaO] = (Ca) + (O)$	1049±1
$[TiO_2] = (TiO_2)$	595±1
$[CaTiO_3] = (CaTiO_3)$	1030±22
$(CaO) + (TiO_2) = (CaTiO_3)$	-298±30
$(Ca) + (Ti) + 3(O) = (CaTiO_3)$	-1983±81

The partial pressure values of these molecules increased in 10^2 – 10^3 times on temperature interval 200–300 degrees. It was observed that the rate of the increase was higher for the complicated molecular forms than for simple atom or molecular forms. For example, the data of

mullite vaporization showed that the increase of AlSiO partial pressure was higher than partial pressures Al and SiO: in the temperature interval 1933–2033 K partial pressures Al and SiO increased in ~6 times while AlSiO partial pressure increased in ~16 times

[Shornikov et al., 1994]. It is interesting to note that such regularities have been fixed on MgO, CaO, SiO₂, Al₂O₃ vaporizations when molecular forms in gaseous phase increased with temperature increase [Kulikov, 1969]. For example, the MgO dissociation level in temperature interval 1400–3000 K decreased from 0.9 to 0.3 and the CaO dissociation level in temperature interval 1800–3200 K decreased from 0.4 to 0.25. The same regularities was noted for SiO₂ and Al₂O₃ oxides when molar doles of SiO suboxide and Al atomic forms decreased with temperature increase as well as more complicated molecular SiO₂ and suboxide AlO, Al₂O, Al₂O₂ forms increased.

The question arises why the contents of complicated molecules increase when the temperature increases? The reason necessary to find in the enthalpy values of the vaporization reactions (table 1).

The table data show the enthalpy values $\Delta H_r(T)$ of these reactionary vaporization from condense phases are positive and have very high meanings. The forming reactions for complicated molecules from the gaseous atoms and simple molecules have negative meaning. The connection formula between $\Delta H_r(T)$, temperature and equilibrium constant of reactions has form:

$$\frac{d \ln K_r(T)}{d(1/T)} = -\frac{\Delta H_r(T)}{R}, \quad (1)$$

where R is gaseous constant. This formula is famous Vant-Goff equation showing that equilibrium constant of reactions in dependence on temperature is conditioned by value of $\Delta H_r(T)$ and the minus (plus) sign of the enthalpy.

The ratio $\frac{d \ln K_r(T)}{d(1/T)}$ is positive for exothermic reactions

($\Delta H_r(T) < 0$) and negative for endothermic reactions ($\Delta H_r(T) > 0$). The negative ratio means that the $K_r(T)$ value is increasing with temperature increase that in turn means equilibrium to reactionary products. In the case exothermic reactions the situation is opposite [Atkins, 1980]. The Vant-Goff equation permit to do two conclusions:

1) The positive enthalpy of the heterogeneous vaporization reactions must be reflected on the $\ln K_r(T) - 1/T$ diagram by negative bended lines. It is necessary to note that the enthalpy sign uncovers the mechanism of complicated molecules origin. If complicated molecules formed in gaseous phase reactions, which are exothermic (these reaction marked blue color in table 1), the dependence lines on $\ln K_r(T) - 1/T$ diagram might be positive bend that did not observe in the experiments. Therefore it is possible to conclude that the origin of complicated molecules: AlSiO, MgAlO and CaTiO₃ was resulted just in heterogeneous reactions but not in reactions in gaseous phase.

2) The Vant-Goff equation shows that the lines on $\ln K_r(T) - 1/T$ diagram must have larger bend for heterogeneous reactions which have larger enthalpy values. In the table for comparison there are enthalpies both the complicated molecules and simple atomic and molecular particles. It's possible to see that the forming enthalpies for simple molecules are less then for complicated ones. Therefore the bends on $\ln K_r(T) - 1/T$ diagram for vaporization reaction of simple molecules are visible less. In consequence the complicated molecules contents in gaseous phase are becoming larger.

References:

1. Atkins, P. W. (1980). Physical chemistry. M.: Mir, vol. 1, 580 p.
2. Chase, M. W. (1998). NIST-JANAF Thermochemical Tables. *J. Phys. Chem. Ref. Data*, Monograph no. 9, pp. 1–1951.
3. Kulikov, I. S. (1969). Thermal dissociation of compounds. M.: Metallurgiya, 576 p. [in Russian].
4. Shornikov, S. I. (2001). Vaporization processess and thermodynamic properties of magnesium aluminate. *Proc. X Russian conference «Structure and properties of metallic and slag melts»*, vol. 3, pp. 73–76 [in Russian].
5. Shornikov, S. I. (2013). Vaporization processess and thermodynamic properties of perovskite CaTiO₃. *A modern problems of theoretical, experimental and applied mineralogy*. Syktyvkar. pp. 367–368 [in Russian].
6. Shornikov, S. I., V. L. Stolyarova, M. M. Shultz (1994). High temperature mass spectrometric study of 3Al₂O₃·2SiO₂. *Rapid Commun. Mass Spectr.*, v. 8, no. 5, pp. 478–480.